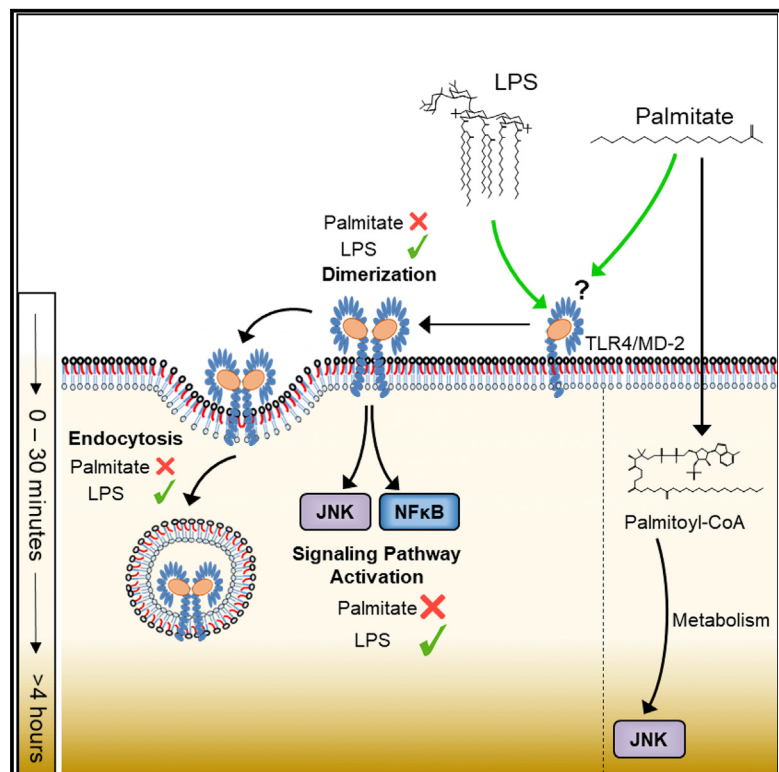


Cell Metabolism

Evidence that TLR4 Is Not a Receptor for Saturated Fatty Acids but Mediates Lipid-Induced Inflammation by Reprogramming Macrophage Metabolism

Graphical Abstract



Authors

Graeme I. Lancaster,
Katherine G. Langley,
Nils Anton Berglund, ..., Peter J. Meikle,
Peter J. Bond, Mark A. Febbraio

Correspondence

graeme.lancaster@baker.edu.au (G.I.L.),
m.febbraio@garvan.org.au (M.A.F.)

In Brief

Saturated fatty acids are believed to be TLR4 agonists, promoting macrophage activation and obesity-associated inflammation. Lancaster et al. demonstrate that the inflammatory fatty acid palmitate is actually not a TLR4 agonist. TLR4 is, however, required for palmitate-induced inflammation through TLR4-dependent priming and altered cellular metabolism, thus reconciling discordant observations.

Highlights

- The long-chain saturated fatty acid palmitate is not a TLR4 agonist
- Palmitate is unable to activate JNK in TLR4-deficient macrophages
- Priming TLR4-deficient macrophages restores palmitate's inflammatory effects
- Priming requires mTOR and is associated with altered lipid metabolism and ER stress

Evidence that TLR4 Is Not a Receptor for Saturated Fatty Acids but Mediates Lipid-Induced Inflammation by Reprogramming Macrophage Metabolism

Graeme I. Lancaster,^{1,2,11,*} Katherine G. Langley,^{1,10,11} Nils Anton Berglund,³ Helene L. Kammoun,¹ Saskia Reibe,⁴ Emma Estevez,⁴ Jacquelyn Weir,¹ Natalie A. Mellett,¹ Gerard Pernes,¹ James R.W. Conway,^{4,5} Man K.S. Lee,¹ Paul Timpton,^{4,5} Andrew J. Murphy,^{1,2} Seth L. Masters,^{6,9} Steve Gerondakis,^{7,10} Nenad Bartonicek,⁴ Dominik C. Kaczorowski,⁴ Marcel E. Dinger,^{4,5} Peter J. Meikle,¹ Peter J. Bond,^{3,8} and Mark A. Febbraio^{1,4,5,12,*}

¹Baker Heart and Diabetes Institute, 75 Commercial Road, Melbourne, VIC 3004, Australia

²Department of Immunology, Monash University, Melbourne, VIC 3004, Australia

³Bioinformatics Institute (A*STAR), 30 Biopolis Street, #07-01 Matrix, Singapore 138671, Singapore

⁴Garvan Institute of Medical Research, 384 Victoria St, Sydney, NSW 2010, Australia

⁵Faculty of Medicine, St Vincent's Clinical School, Faculty of Medicine, University of NSW, Sydney, NSW 2010, Australia

⁶Inflammation Division, The Walter and Eliza Hall Institute of Medical Research, Parkville, VIC 3052, Australia

⁷Biomedicine Discovery Institute, Monash University, Clayton, VIC 3800, Australia

⁸Department of Biological Sciences, National University of Singapore, 14 Science Drive 4, Singapore 117543, Singapore

⁹Department of Medical Biology, The University of Melbourne, Parkville, VIC 3010, Australia

¹⁰Department of Biochemistry and Molecular Biology, Monash University, Clayton, VIC 3800, Australia

¹¹These authors contributed equally

¹²Lead Contact

*Correspondence: graeme.lancaster@baker.edu.au (G.I.L.), m.febbraio@garvan.org.au (M.A.F.)

<https://doi.org/10.1016/j.cmet.2018.03.014>

SUMMARY

Chronic inflammation is a hallmark of obesity and is linked to the development of numerous diseases. The activation of toll-like receptor 4 (TLR4) by long-chain saturated fatty acids (lcSFAs) is an important process in understanding how obesity initiates inflammation. While experimental evidence supports an important role for TLR4 in obesity-induced inflammation *in vivo*, via a mechanism thought to involve direct binding to and activation of TLR4 by lcSFAs, several lines of evidence argue against lcSFAs being direct TLR4 agonists. Using multiple orthogonal approaches, we herein provide evidence that while loss-of-function models confirm that TLR4 does, indeed, regulate lcSFA-induced inflammation, TLR4 is not a receptor for lcSFAs. Rather, we show that TLR4-dependent priming alters cellular metabolism, gene expression, lipid metabolic pathways, and membrane lipid composition, changes that are necessary for lcSFA-induced inflammation. These results reconcile previous discordant observations and challenge the prevailing view of TLR4's role in initiating obesity-induced inflammation.

INTRODUCTION

Obesity affects approximately one-third of adults in the Western world and increases the risk of developing a number of chronic diseases, including, but not limited to, type 2 diabetes, cardio-

vascular disease, and certain types of cancer. Chronic, low-grade inflammation plays a central role in the development of numerous obesity-related diseases (Brestoff and Artis, 2015), and identifying the proximal events that initiate obesity-induced inflammation is of major therapeutic importance.

Pattern-recognition receptors (PRRs) are key components of the host immune system, facilitating the recognition of pathogen- and damage-associated molecular patterns (Takeuchi and Akira, 2010). The activation of PRRs initiates inflammatory signaling and gene transcription, responses required for effective clearance of the initiating insult (Takeuchi and Akira, 2010). Importantly, several PRRs are also proposed to "sense" nutrient excess, notably specific lipids, thereby providing a mechanistic link between obesity and inflammation (Hotamisligil, 2017).

Toll-like receptor (TLR) 4 is the best characterized of all PRRs. The earliest evidence linking TLR4 to lipid-induced inflammation predates its identification as the receptor for LPS (Liao et al., 1993). More recent *in vitro* and *in vivo* studies (Caesar et al., 2015; Huang et al., 2012; Jia et al., 2014; Lee et al., 2001; Nagareddy et al., 2014; Nguyen et al., 2007; Pal et al., 2012; Saberi et al., 2009; Shi et al., 2006) have confirmed these earlier findings, and the activation of TLR4 by lipids has become an important paradigm for understanding how obesity initiates inflammation (Hotamisligil, 2017; McNelis and Olefsky, 2014).

Mechanistically, it is hypothesized that long-chain saturated fatty acids (lcSFAs) are TLR4 agonists (Osborn and Olefsky, 2012). In general support of this idea, the principal component of LPS responsible for its immunostimulatory activity is the lipid A (LPA) region, which contains numerous saturated fatty acyl chains that are required for binding to and activating TLR4. However, while the binding of lcSFAs to TLR4 is an intuitively

appealing idea, several lines of evidence argue against IgSFAs being TLR4 agonists. First, most (Gallic et al., 2011; Hernandez et al., 2014; Holzer et al., 2011; Jaeschke and Davis, 2007; Nguyen et al., 2007), although not all (Huang et al., 2012; Shi et al., 2006), previous studies demonstrate that IgSFAs take several hours to initiate inflammatory signaling; in contrast, LPS activates inflammatory signaling within minutes. Second, while the inflammatory effects of fatty acids are confined to IgSFAs, myeloid differentiation factor 2 (MD-2), which physically interacts with TLR4 and is principally responsible for ligand binding via its hydrophobic pocket, is able to bind fatty acyl chains of variable length and saturation status. Finally, it would appear counterintuitive for circulating IgSFAs, which fluctuate physiologically, to activate such a potent inflammatory pathway. Nonetheless, numerous published studies provide compelling evidence that TLR4 regulates obesity-induced inflammation and metabolic dysfunction. Herein, using numerous complementary experimental approaches, we demonstrate that IgSFAs are not TLR4 agonists. Instead, we provide evidence that TLR4 indirectly regulates IgSFA-induced inflammation by altering macrophage lipid metabolism. These results shed light on the precise role of TLR4 in obesity-induced inflammation *in vivo*.

RESULTS

Molecular Simulations of TLR4₂/MD-2₂ with Palmitate Provide Evidence that Palmitate Is Not a TLR4 Agonist

Although TLR4 is often considered the receptor for LPS, MD-2, a co-receptor that physically interacts with the extracellular domain of TLR4, is principally responsible for LPS binding (Park et al., 2009). In the inactive state, TLR4 exists as a heterodimer with MD-2. The binding of LPS to TLR4/MD-2 creates a dimerization interface that facilitates the formation of the active complex consisting of a “dimer of dimers” (TLR4₂/MD-2₂), arranged symmetrically in an M-like shape (Park et al., 2009) (Figure S1A). As per convention, the second TLR4/MD-2 complex is indicated with an asterisk to distinguish it from the primary TLR4/MD-2 complex. The F126 loop of MD-2 is particularly important in stabilizing the active TLR4₂/MD-2₂ complex, undergoing a significant structural shift upon LPS binding (Park et al., 2009). The importance of the F126 loop has been demonstrated experimentally as an F126A MD-2 mutant has a markedly reduced capacity to form the active TLR4₂/MD-2₂ complex and to activate downstream signaling pathways (Tan et al., 2015). Using atomically detailed molecular dynamics (MD) simulations, we previously demonstrated that F126 acts as a molecular switch, adopting a “closed” conformation that points inside the MD-2 cavity in the presence of LPS, thereby promoting stability of the active TLR4₂/MD-2₂ complex (Paramo et al., 2013). In contrast, in the absence of agonist, or in the presence of partial agonists (e.g., monophosphorylated lipid A [MPLA]) or antagonists (e.g., Eritoran), F126 adopts an “open” conformation, which physically disrupts the dimerization interface and hence destabilizes the TLR4₂/MD-2₂ complex (Paramo et al., 2013, 2015).

To gain insight into the potential for IgSFAs to act as TLR4/MD-2 agonists, we have used MD simulations to determine the effects of the IgSFA palmitate on conformational changes in the F126 gating loop as well as on the stability of the complete, active TLR4₂/MD-2₂ complex (background discussion to this

approach is provided in the STAR Methods). To maximize the likelihood of achieving a physiological mode of lipid binding and of observing an agonistic effect, we performed MD simulations of palmitate with the TLR4₂/MD-2₂ complex under the following conditions: (1) five palmitate molecules were aligned within the lipid-binding hydrophobic pocket of MD-2 based on the position of the acyl chains of hexa-acylated LPS in the X-ray structure of TLR4₂/MD-2₂ (Park et al., 2009), and (2) three palmitate molecules were aligned within the lipid-binding hydrophobic pocket of MD-2 based on the position of the three endogenous myristate molecules that were previously observed to co-crystallize with native MD-2 (Ohto et al., 2007). To assess shifts in conformation of the F126 loop, β strands of MD-2 from the simulated active TLR4₂/MD-2₂ complex were aligned onto the X-ray structure to determine the pairwise root-mean-square deviation (RMSD) of the Cα atoms of the F126 loop. This measure provides an assessment of the shift in the F126 loop relative to the rest of the protein (Paramo et al., 2013). For TLR4₂/MD-2₂ in complex with LPA, the RMSD was ~0.2 nm and the F126 loop maintained the closed conformation necessary for the stability of the active TLR4₂/MD-2₂ complex (Figures 1A–1C). In contrast, the 3× and 5× palmitate systems destabilized the closed gating loop conformation with an RMSD of ~0.3–0.4 nm (Figures 1A–1C), comparable with the apo state; i.e., the absence of ligand.

We have previously shown that the switch of the F126 loop from a closed to open conformation destabilizes the active TLR4₂/MD-2₂ complex due to the loss of key interaction interfaces (Paramo et al., 2013). Accordingly, we examined the stability of the active TLR4₂/MD-2₂ complex in the context of key interactions at the primary (between TLR4 and MD-2) and secondary (between TLR4* and MD-2) interfaces. Prior to LPS binding, interactions between TLR4 and MD-2 occur at the primary interface and these are largely unaffected by LPS binding (Park et al., 2009). Consistently, following simulation, interactions at the primary interface were well maintained, displaying a constant buried surface area in the presence of either 3× palmitate, 5× palmitate, LPA, or in the unbound apo state (Figures 1D and 1E). These results are consistent with experimental observation (Park et al., 2009) and our own previous findings (Paramo et al., 2013). However, interactions at the secondary interface, which are critical for dimerization of TLR4/MD-2, were destabilized in the 3× and 5× palmitate systems, leading to a significant loss of buried surface area (Figures 1D and 1F). The 1-phosphate group of LPA has an important role in stabilizing the dimerization interface through interactions with K388* of TLR4* and this interaction was absent in the 3× and 5× palmitate systems (Figures 1D and 1G). The secondary interface in the TLR4₂/MD-2₂-LPA system was stable and reproduced key interactions present in the crystal structure of TLR4/MD-2 bound to LPS as well as our own previous simulations of TLR4₂/MD-2₂-LPA (Paramo et al., 2013) (Figures 1D and 1G).

Collectively, these data demonstrate that simulations of 3× and 5× palmitate within the active TLR4₂/MD-2₂ receptor complex leads to reorientation of the F126 loop from the closed to open conformation and destabilization of the key dimerization interface between MD-2 and TLR4*. To determine whether the loss of stability at the dimerization interface would lead to an overall loss of receptor stability, we calculated pairwise RMSDs between the Cα atoms of components of the active receptor

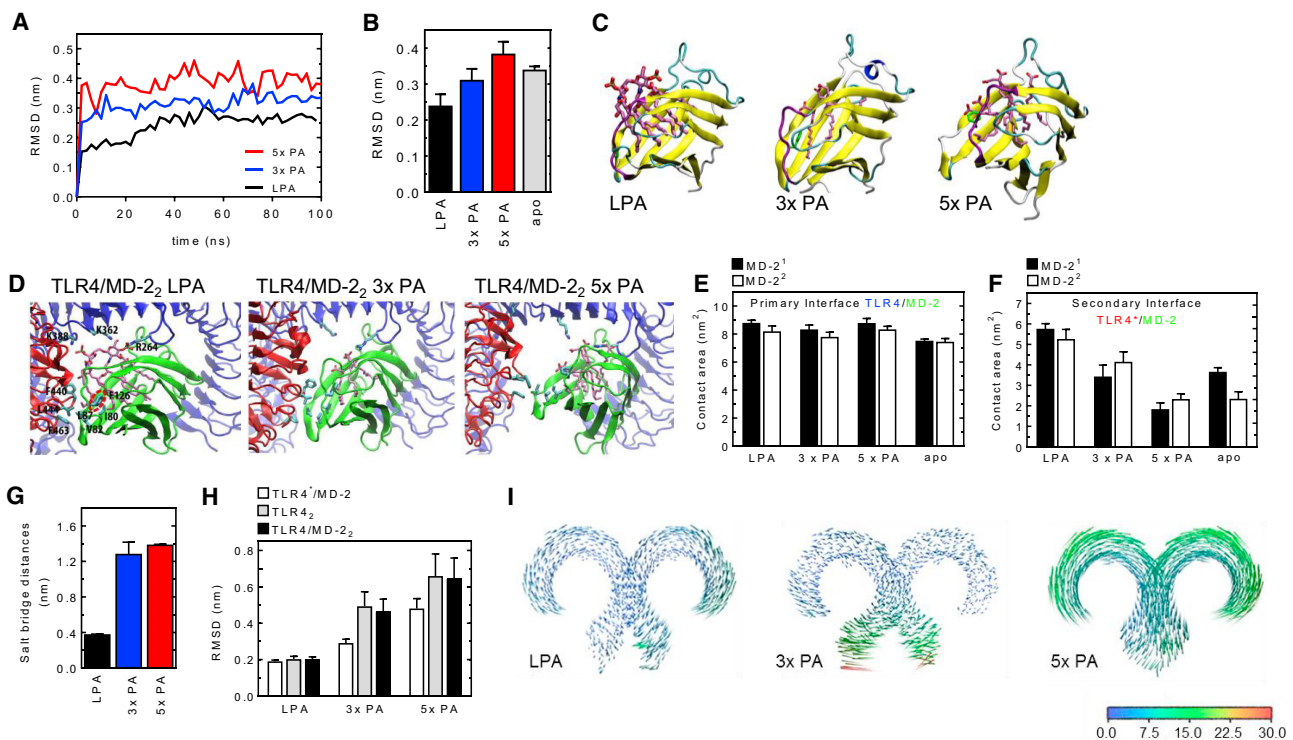


Figure 1. Molecular Simulations of the TLR4/MD-2 Active Complex Provide Evidence that Palmitate Is Not a TLR4 Agonist

(A–C) RMSD of the F126 gating loop in MD-2 throughout 100 ns simulations of LPA, 3x palmitate (PA), or 5x PA bound to the activated receptor complex, relative to the X-ray structure (A), and the average values over the final 20 ns of each simulation (B). In (C), the final confirmation of the F126 loop is shown. MD-2 is shown in schematic format, F126 (green) and ligand shown in wireframe format. The gating loop is highlighted in purple.

(D) The final simulation structure of the complex when bound to LPA (left panel), 3x PA (middle panel), and 5x PA (right panel). Protein chains are marked as follows: TLR4 (blue), TLR4* (red), and MD-2 (green). MD-2* is not shown. LPA and PA ligands are shown in wireframe format. Key interacting residues are labeled in the LPA simulation structure. The orientation of F126 is highlighted with a red dashed ellipse in the LPA simulation structure.

(E and F) The mean contact surface area buried between MD-2 and TLR4 at the primary (E) and secondary (F) interfaces was calculated over the final 20 ns, each shown for the two equivalent sites within the overall receptor complex.

(G) Distance between the 1-phosphate group of LPA or the nearest carboxyl group of a PA molecule to K388* in TLR4* calculated from the final simulation structure.

(H) Mean C_α RMSD for the indicated chains over the final 20 ns of simulations of the active receptor complex relative to the X-ray structure.

(I) Principal component analysis of both TLR4 chains in the complex when bound to LPA, 3x PA, and 5x PA (the MD-2 chains are omitted for clarity). The dominant, collective mode of motion for each C_α atom is represented by an arrow, with the magnitudes of motion indicated by arrow length and color according to the inset key, in distance units of Ångströms.

The data in (I) were plotted using VMD (visual molecular dynamics) (Humphrey et al., 1996) and represent an interpolation between the two extreme projections around the average TLR4 structure, after projection of the trajectory onto the first eigenvector. Data in (B) and (E)–(H) are shown as the mean ± SEM of the RMSD over the final 20 ns of simulation.

complex and the X-ray structure of the active TLR4/MD-2-LPS complex. Compared with the LPA-bound state, the 3x and 5x palmitate systems displayed considerable divergence (~ 0.2 – 0.4 nm) from the X-ray structure of the active TLR4/MD-2-LPS complex, indicative of instability of the receptor complex, effects that were comparable with the apo state (Figure 1H).

Ligand-induced conformational changes that bring the C-terminal regions of TLRs together are likely to be important for the activation of downstream signaling. We hypothesized that the loss of receptor stability in the 3x and 5x palmitate systems may lead to separation of the membrane-proximal C-terminal regions of TLR4. To test this, we performed principal component analysis for the TLR4 C_α atoms, in order to filter the “noise” from the trajectory and identify the dominant collective motions of the receptor chains. In simulations of the active TLR4₂/MD-2₂ complex with 3x palmitate, we observed a horizontal

separating motion of the two TLR4 chains (Figure 1I). In the case of the 5x palmitate system, an even more dramatic, vertical sliding motion between chains was observed (Figure 1I). Both of these patterns of motion would lead to a loss of proximity of the membrane-proximal C-terminal regions and inactivation of the receptor complex. In contrast, simulations of TLR4₂/MD-2₂-LPA revealed no significant “separating” motions of TLR4 chains, consistent with stabilization of the complex when bound to agonist (Figure 1I).

Finally, we noticed that, compared with the X-ray structure of TLR4₂/MD-2₂ bound to LPS, in the presence of either 3x or 5x palmitate an “outward” shift of ~ 10 Å of MD-2 occurred relative to TLR4 as it disassembled from TLR4* during simulation (Figure S1B). Importantly, this shift in MD-2 appears to be physiologically relevant, as this shifted conformation closely resembles the X-ray structure of both the murine TLR4/MD-2 heterodimer in the

inactive, unliganded state, and of human TLR4/MD-2 bound to Eritoran, a TLR4 antagonist (Kim et al., 2007). Collectively, the MD simulations demonstrate that the presence of three or five palmitate molecules within the active TLR4₂/MD-2₂ receptor complex leads to destabilization of the receptor complex and, therefore, do not support the idea that IcSFAs are direct agonists of TLR4.

Palmitate and LPS Induce Distinct Profiles of Signaling Pathway Activation

LPS, the canonical TLR4 agonist, induces a rapid and prototypical signaling response that includes the activation of mitogen-activated protein kinases (MAPKs), nuclear factor κB (NF-κB), and interferon regulatory factors (IRFs) (Hoebe et al., 2003; Horng et al., 2002; Wang et al., 2016; Yamamoto et al., 2002, 2003). We reasoned that if palmitate is a *bona fide* TLR4 agonist, it should induce a similar profile of signaling pathway activation to LPS. Accordingly, we compared the activation of NF-κB and JNK signaling pathways in primary bone marrow-derived macrophages (BMDMs) from C57Bl6/J (wild-type [WT]) mice in response to the canonical TLR4 agonist LPS and the IcSFA palmitate. BMDMs were generated by culturing bone marrow cells in L-cell-containing media (LCM) for 7 days. To minimize any potentially confounding effects that serum components or BSA, to which fatty acids are conjugated and which is used in almost all studies in which exogenous fatty acids are added to cells, may have on signaling pathway activation (Erridge, 2010; Erridge and Samani, 2009; Pal et al., 2012), after 7 days of LCM stimulation, differentiated BMDMs were cultured overnight in media containing FBS and BSA (i.e., the media used for treating BMDMs, but without fatty acids) prior to treatment with either fatty acids or vehicle control. Importantly, our results using this protocol replicate the effects of palmitate reported in numerous published studies, including increased JNK phosphorylation, TNF release (Figure S2A), and endoplasmic reticulum (ER) stress (Figures 7A–7C), as well as dose dependency (Figure S2D) and time course responses (Figure 2E). Furthermore, consistent with their reported activities, the SFA myristate (14:0) and long-chain unsaturated fatty acid palmitoleate (16:1) were unable to induce TNF release or JNK phosphorylation (Figures S2B, S2C, and S2E).

As expected, treatment with LPS induced rapid JNK and MKK4/7 phosphorylation as well as the phosphorylation of p65 and the degradation of IκB α , indicative of canonical NF-κB activation (Figures 2A–2D). In contrast to the effects of LPS, palmitate-induced JNK and MKK4/7 phosphorylation occurred only after 4 hr of treatment (Figures 2E and 2F), and we observed no evidence of NF-κB activation over the course of the experiment (Figures 2G and 2H). Consistent with published literature, palmitate induced TNF release (Figure S2A), although this effect was ~20-fold lower than for LPS (Figure S2A). The rapid activation of MAPK and NF-κB signaling pathways is a hallmark of TLR activation. These data, therefore, provide evidence that the IcSFA palmitate is not activating JNK by directly binding to and activating TLR4. It is possible that IcSFAs such as palmitate activate TLR4 in an unconventional manner, and precedence exists for such an effect. MPLA, a TRIF-biased agonist of TLR4, induces a profile of signaling pathway activation and cytokine production distinct from that of LPS (Mata-Haro et al., 2007).

Palmitate Does Not Induce TLR4 Dimerization or Endocytosis

Ligand-dependent dimerization of TLR4/MD₂ heterodimers leading to formation of the active TLR4₂/MD-2₂ heterotetramer is the most proximal event in the initiation of TLR4 pathway activation. TLR4 dimerization can be monitored *in vivo* with an antibody (MTS510; TLR4/MD-2-PE/Cy7 [R-Phycoerythrin (PE)/Cyanine7(Cy7)]) that is specific for the monomeric form of TLR4 (Tan et al., 2015; Zanoni et al., 2017). Accordingly, the loss of cell surface expression of TLR4 using MTS510 represents both dimerization and the subsequent endocytosis of the active TLR4₂/MD-2₂ complex. The remaining cell surface expression represents monomeric TLR4; i.e., the un-activated TLR4/MD-2 heterodimer. Using this approach, we demonstrate that approximately 80% of TLR4 is dimerized 15 min following treatment of BMDMs with LPS (Figure 3A), consistent with the findings of previous studies (Tan et al., 2015; Zanoni et al., 2017). In contrast, palmitate treatment of BMDMs was unable to induce TLR4 dimerization (Figure 3A). The activation-induced dimerization of TLR4 leads to its internalization into endosomes via endocytosis, a critical event in TLR4 pathway activation (Zanoni et al., 2011). Using an antibody (Sa15-21; TLR4-APC; Allophycocyanin [APC]) that recognizes TLR4 regardless of its activation state (i.e., both monomeric and dimeric TLR4), ligand-induced endocytosis of TLR4 can be monitored (Zanoni et al., 2011). Accordingly, we compared the endocytosis of TLR4 in BMDMs treated with either LPS or palmitate. While LPS induced the previously described time-dependent endocytosis of TLR4 (Zanoni et al., 2011), palmitate did not induce detectable TLR4 endocytosis over the course of the experiment (Figure 3B). Collectively, these results support the data from MD simulations and signaling experiments, and provide further evidence that palmitate is not an agonistic ligand for TLR4.

Acute Pharmacological Inhibition of TLR4 Does Not Prevent Palmitate-Induced Activation of JNK

The preceding data do not support the concept that IcSFAs such as palmitate are TLR4 agonists. To further examine if palmitate is a TLR4 agonist, we employed two structurally unrelated inhibitors of TLR4 activation, each with a distinct mechanism of action. LPS variants containing fewer than six acyl chains in their lipid A region bind to TLR4/MD-2 but are weak inducers of dimerization and TLR4-dependent signaling (Tan et al., 2015). For example, penta-acylated LPS from *Rhodobacter sphaeroides* (LPS-Rs) is a strong antagonist of *Escherichia coli* LPS-induced myddosome formation and TLR4-dependent gene expression (Tan et al., 2015). Accordingly, we pre-treated BMDMs with LPS-Rs for 1 hr prior to stimulating with either LPS-*E. coli* (LPS-Ec) or palmitate. As expected, we observed that LPS-Rs completely prevented LPS-Ec-induced JNK phosphorylation (Figure 4A). In contrast, LPS-Rs was unable to prevent palmitate-induced JNK phosphorylation (Figure 4B). Because LPS-Rs competitively inhibits TLR4-dependent signaling by binding within the hydrophobic pocket of MD-2, it is possible that palmitate may activate TLR4 independently of binding the MD-2 lipid-binding pocket. Indeed, nickel and cobalt activate TLR4 in an MD-2-independent manner (Raghavan et al., 2012). To address this issue, we used a second inhibitor, TAK-242, which binds to C747 within the intracellular

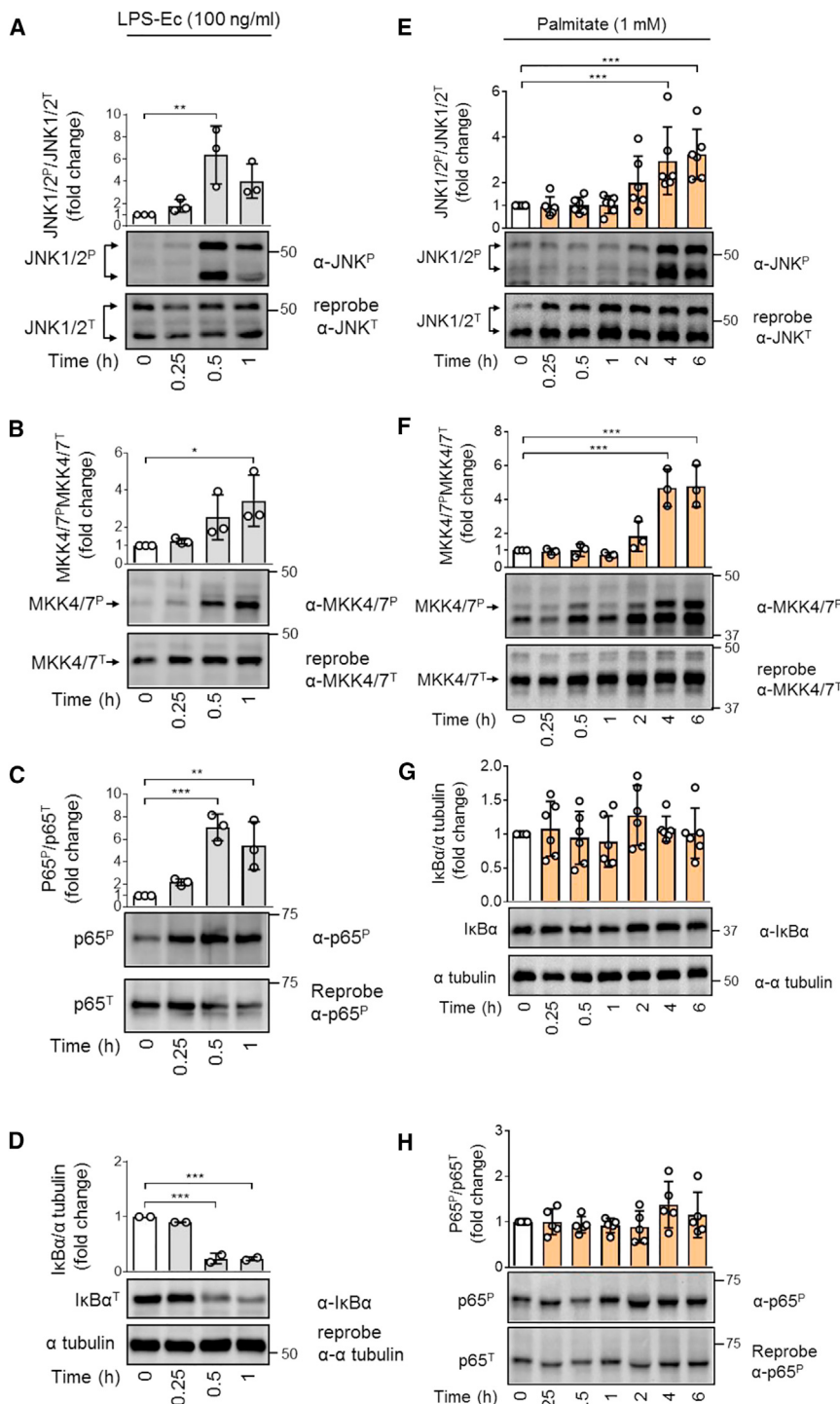


Figure 2. Palmitate and LPS-Ec Activate Distinct Signaling Pathways in BMDMs

WT BMDMs were treated with either LPS-*Escherichia coli* (LPS-Ec) (100 ng/mL) (A–D) or palmitate (1 mM) (E–H) for the indicated durations. Cell lysates were analyzed by immunoblotting for levels of phosphorylated (^P) and total (^T) JNK1/2 (A and E), MKK4/7 (B and F), p65 (C and G), and IκBα and α tubulin (D and H). The following numbers of biological replicates (independent mice) were used in each experiment: (A)–(C) = 3; (D) = 2; (E), (G), and (H) = 6; (F) = 3. All experiments were performed in either technical duplicates or triplicates and averaged such that for each independent experiment $n = 1$. All data are expressed as the mean \pm SD and are expressed as a fold change from the 0 time point. Symbols within bars represent the average value of each biological replicate. Asterisks represent statistical significance at the following α levels: *** $p < 0.001$; ** $p < 0.01$; * $p < 0.05$.

greater than was required to maximally inhibit LPS-Ec-induced JNK phosphorylation (Figures 4C and 4D). Some differences exist in the capacity of specific ligands to activate human and rodent TLR4 (Lien et al., 2000; Raghavan et al., 2012). We therefore assessed whether TLR4 was required for palmitate-induced JNK phosphorylation in primary human peripheral blood monocyte-derived macrophages (HMDMs). Similar to BMDMs, palmitate-induced JNK phosphorylation in HMDMs was independent of TLR4 (Figures 4E and S2F). As expected, LPS-Ec-induced JNK phosphorylation in HMDMs was completely dependent on intact signaling via TLR4 (Figures 4F and S4G). Collectively, these data demonstrate that blocking TLR4 signaling does not prevent LCFA-induced JNK activation.

Consistent with previous literature documenting a role for TLR4 in palmitate-induced inflammation (Huang et al., 2012; Lee et al., 2001; Nguyen et al., 2007; Pal et al., 2012; Shi et al., 2006), we found that palmitate-induced JNK phosphorylation, similar to LPS-induced JNK phosphorylation, was abolished in BMDMs from *Tlr4*^{-/-} mice (Figures 4G and S2H). Near identical results were ob-

TIR domain of TLR4, is highly selective for TLR4, and inhibits both MyD88- and TRIF-dependent signaling (Takashima et al., 2009). Pre-treatment of BMDMs for 1 hr with TAK-242 completely prevented JNK phosphorylation upon exposure to LPS-Ec (Figure 4C), whereas, in contrast, pre-treatment of BMDMs for 1 hr with TAK-242 failed to prevent palmitate-induced JNK phosphorylation, even at concentrations ten times

obtained in BMDMs from C3H/HeJ mice (Figure 4H), which harbor a mutation in the TIR domain of TLR4 that results in defective LPS signaling but normal TLR4 expression (Poltorak et al., 1998). Control BMDMs obtained from C3H/HeN mice demonstrated robust JNK phosphorylation following palmitate treatment (Figure 4H). These results confirm that TLR4 is required for LCFA to elicit their pro-inflammatory effects.

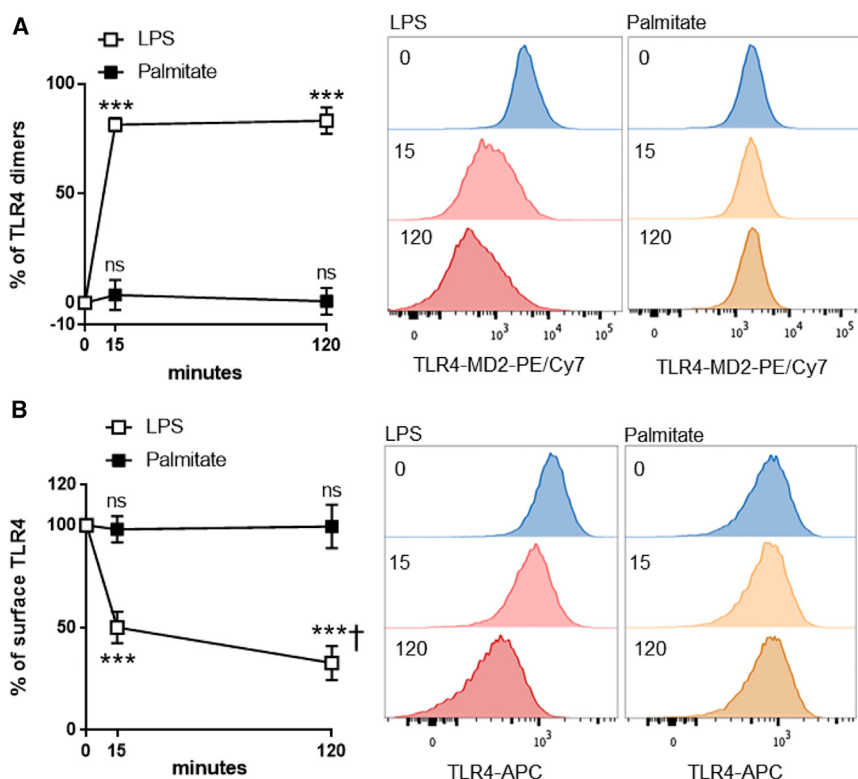


Figure 3. Palmitate Is Unable to Induce TLR4 Dimerization or Endocytosis

(A and B) WT BMDMs were treated with either LPS-Ec (1 µg/mL) or palmitate (1 mM) for the indicated durations and TLR4 dimerization (A) and endocytosis (B) were determined by flow cytometry. Line graphs represent the mean ± SD from seven biological replicates (independent mice). Asterisks represent statistical significance at the following α levels: *** p < 0.001 versus 0; $^{\dagger}p$ < 0.005 versus 15.

Priming of *Tlr4*^{-/-} and C3H/HeJ BMDMs with TLR2 or TLR3 Agonists Restores Sensitivity to Palmitate

Collectively, our results raise an intriguing paradox: IcSFAs such as palmitate are not TLR4 ligands, yet deletion of TLR4 abolishes their inflammatory actions. Accordingly, we hypothesized that TLR4 indirectly mediates IcSFA-induced inflammation. Specifically, given that serum components and BSA have been linked to TLR4 activation, we considered the possibility that the cell culture conditions, specifically the pre-treatment media, may activate TLR4, thereby priming BMDMs such that subsequent exposure to IcSFAs activated inflammatory signaling. TLR4-dependent priming in WT BMDMs would account for both the inability of palmitate to induce JNK phosphorylation in *Tlr4*^{-/-} BMDMs and our observations that palmitate is not a direct TLR4 agonist. To address this hypothesis, RNA sequencing (RNA-seq) was used to examine the expression of known TLR4-activated primary and secondary response genes (Tong et al., 2016) in WT BMDMs that remained in LCM (control-WT BMDMs) or were exposed to pre-treatment media for 6 hr (pre-treated WT BMDMs) (Figures 5A and S3). Compared with control-WT BMDMs, pre-treated WT BMDMs had a marked upregulation in the expression of nearly all of the 226 genes examined (Figures 5A and S3). Altered gene expression was entirely TLR4 dependent, as this effect was abolished in pre-treated *Tlr4*^{-/-} BMDMs (Figures 5A and S3).

These data led us to make two predictions: first, that inhibition of TLR4 signaling prior to switching from LCM to pre-treatment media would prevent palmitate-induced JNK phosphorylation in WT BMDMs, and second, that priming *Tlr4*^{-/-} BMDMs with agonists of alternate TLRs would restore the sensitivity of *Tlr4*^{-/-}

BMDMs to palmitate. To test the first prediction, we extended the conditions of the experiment we performed in Figure 4D, treating WT BMDMs with TAK-242 for 1 hr prior to switching from LCM as well as during the overnight pre-treatment (Figure S4A). BMDMs were subsequently stimulated with palmitate in the absence of TAK-242. Consistent with our hypothesis, inhibition of TLR4 prior to pre-treatment abolished palmitate-induced JNK phosphorylation in WT BMDMs (Figure 5B). TLR4-dependent activation of gene expression is dependent on MyD88-dependent and TRIF-dependent signaling pathways. Therefore, to test

the second prediction, WT and *Tlr4*^{-/-} BMDMs were pre-treated with media containing Pam3CSK4 (a TLR2-MyD88 agonist), polyinosinic:polycytidyllic acid (poly(I:C); a TLR3-TRIF agonist), or vehicle control (Figure S4B). Consistent with our previous data, palmitate-induced JNK phosphorylation was abolished in unprimed *Tlr4*^{-/-} BMDMs (Figure 5C). Remarkably, both Pam3CSK4- and poly(I:C)-induced priming restored the sensitivity of *Tlr4*^{-/-} BMDMs to palmitate (Figure 5C). This was not due to a re-sensitization of *Tlr4*^{-/-} BMDMs to TLR4 agonists, as *Tlr4*^{-/-} BMDMs primed with Pam3CSK4 remained insensitive to LPS (Figure 5D). Re-sensitization to palmitate was also observed in C3H/HeJ BMDMs primed with Pam3CSK4 (Figure 5E). These results demonstrate that the sensitivity of BMDMs to the inflammatory effects of IcSFAs is dependent upon the underlying activation state of the cell. In support of this idea, the priming-induced re-sensitization of *Tlr4*^{-/-} BMDMs to palmitate was associated with a reprogramming of the gene expression landscape toward that observed in WT BMDMs (Figures 5A and S3). These data provide an explanation for the observations that IcSFAs are not TLR4 agonists, yet *Tlr4*^{-/-} BMDMs are protected from the inflammatory effects of IcSFAs.

Loss of the NLRP3 Inflammasome Does Not Affect Palmitate-Induced JNK Activation

The above findings raise the question of how priming and the subsequent changes in the gene expression landscape mediate the cellular sensitivity to palmitate. Consistent with activation of TLR4, the RNA-seq analysis revealed that pre-treatment media increased the expression of several genes involved in activating the NLRP3 inflammasome, including Casp1, IL1b, Nlrp3, and IL18,

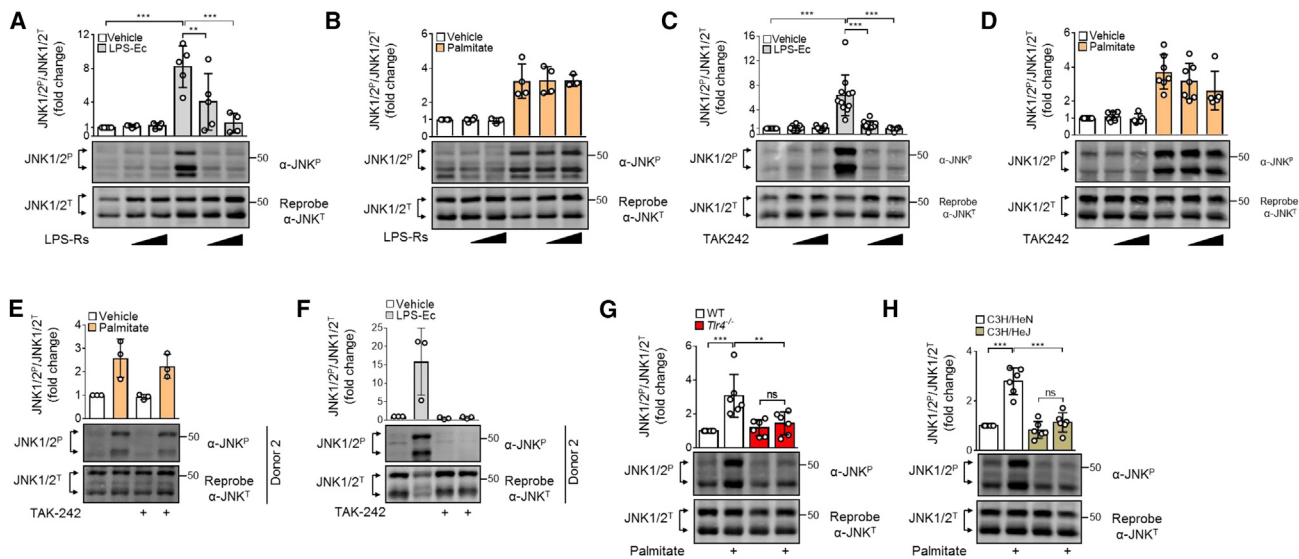


Figure 4. IcSFA-Induced JNK Activation Is Unaffected by Acute Pharmacological Inhibition of TLR4 in BMDMs and HMDMs but Is Abolished in TLR4-Deficient BMDMs

(A–D) WT BMDMs were treated for 1 hr with increasing doses of either LPS-Rs (1 or 10 µg/mL) (A and B) or TAK242 (1 or 10 µM) (C and D), prior to stimulation with either LPS-Ec (100 ng/mL for 0.5 hr) (A and C) or palmitate (1 mM for 4 hr) (B and D). (E and F) HMDMs were treated for 1 hr with 5 µM TAK242 (E and F) prior to stimulation with either palmitate (1 mM for 4 hr) (E) or LPS-Ec (100 ng/mL for 0.5 hr) (F). (G and H) BMDMs from WT and *Tlr4*^{-/-} mice (G) or C3H/HeN and C3H/HeJ mice (H) were stimulated with palmitate (1 mM for 4 hr). Cell lysates were analyzed by immunoblotting for levels of phosphorylated (^P) and total (^T) JNK1/2 (A–H). The following numbers of biological replicates (independent mice) were used in each experiment: (A) = 4–5; (B) = 3–4; (C) = 7–11; (D) = 5–7; (E) and (F) = 3; (G) and (H) = 6. All experiments were performed in either technical duplicates or triplicates and averaged such that for each independent experiment n = 1. All data are expressed as the mean ± SD and are expressed as a fold change. Symbols within bars represent the average value of each biological replicate. Asterisks represent statistical significance at the following α levels: ***p < 0.001; **p < 0.01.

effects that were absent in *Tlr4*^{-/-} BMDMs but were restored in poly(I:C)-primed *Tlr4*^{-/-} BMDMs (Figure S5A). When measured by immunoblotting, the expression of NLRP3 was lower in *Tlr4*^{-/-} BMDMs compared with WT BMDMs and increased following priming with Pam3CSK4 (Figure S5B). Given that IcSFAs activate the NLRP3 inflammasome (Moon et al., 2016; Wen et al., 2011), we considered whether palmitate-induced activation of the NLRP3 inflammasome might mediate palmitate-induced JNK phosphorylation; for example, via autocrine interleukin 1β (IL-1β) signaling. However, palmitate treatment of WT and *Nlrp3*^{-/-} BMDMs, as well as BMDMs deficient in *Pycard* and *Casp1*, critical components of the NLRP3-inflammasome, all resulted in comparable levels of JNK phosphorylation (Figure S5C). Caspase-11 has recently been shown to directly recognize cytoplasmic LPS (Shi et al., 2014). It is, therefore, conceivable that caspase-11 may be activated by the accumulation of specific intracellular lipids that lead to increased JNK activation, potentially via the autocrine actions of IL-1β. However, the *Casp1*^{-/-} BMDMs used herein also lack caspase-11 (Kayagaki et al., 2011), ruling out any role for caspase-11 in mediating IcSFA-induced JNK phosphorylation (Figure S5C).

The Lipidome and Cellular Metabolism of *Tlr4*^{-/-} BMDMs Are Altered Compared with WT BMDMs and Normalized by Priming

Several recent studies have demonstrated that TLR4 activation leads to marked alterations in macrophage metabolism, including increased aerobic glycolysis, a broken TCA cycle,

and the accumulation of succinate (O'Neill et al., 2016). In this regard, it is important to note that altering the metabolic fate of IcSFAs has a major influence on their inflammatory potential. Specifically, channeling IcSFAs into neutral lipids, such as triacylglycerol (Koliwad et al., 2010), or increasing their oxidation decreases palmitate-induced JNK activation (Galic et al., 2011). Furthermore, the lipid composition of cell membranes is altered following TLR4 activation, affecting their biophysical properties and influencing inflammatory signaling (Erbay et al., 2009; Holzer et al., 2011; Köberlin et al., 2015; Rong et al., 2013; Wei et al., 2016). Therefore, in considering how priming may alter BMDM sensitivity to palmitate, we hypothesized that priming-induced metabolic reprogramming may underlie the sensitivity and insensitivity of WT and *Tlr4*^{-/-} BMDMs, respectively, to the inflammatory effects of palmitate. Consistent with the idea that priming induced metabolic reprogramming in WT BMDMs, *Irg1* and *Nos2*, critical mediators of the altered metabolism that occurs in TLR4-activated macrophages and dendritic cells (Everts et al., 2012; Lampropoulou et al., 2016), were two of the most up-regulated genes in pre-treated WT BMDMs (Figures 5A and S3; highlighted with black boxes). Of note, *Irg1* and *Nos2* expression was not increased in *Tlr4*^{-/-} BMDMs but was increased to levels comparable with WT BMDMs in poly(I:C)-primed *Tlr4*^{-/-} BMDMs (Figures 5A and S3). Consistent with these effects, and of the known decrease in fatty acid oxidative capacity in TLR4-stimulated macrophages compared with unstimulated macrophages (Huang et al., 2014), we observed increased rates of ³H-palmitate oxidation and correspondingly lower levels of

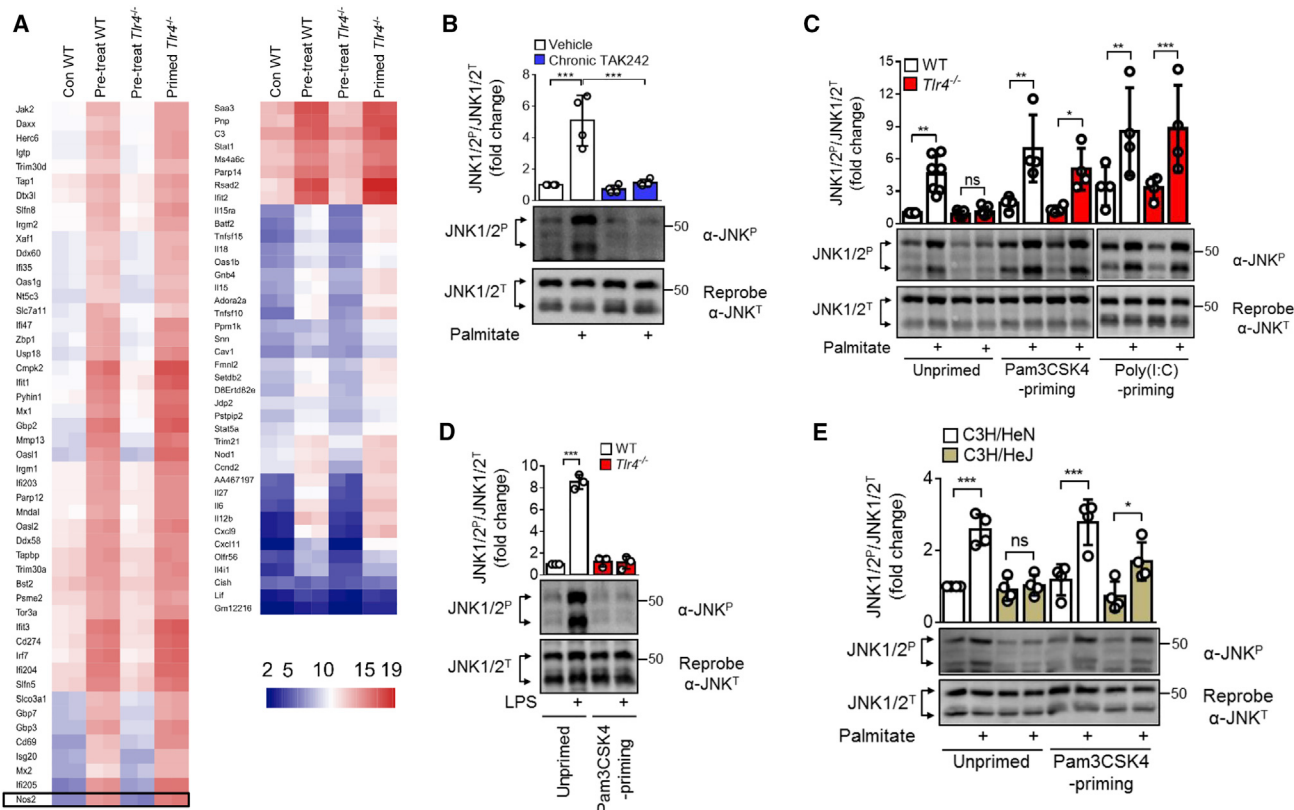


Figure 5. Priming Is Necessary for lcSFA-Induced JNK Activation

(A) RNA-seq analysis of expression of TLR4-activated secondary response genes in WT BMDMs that were untreated and remained in LCM (Con WT), in WT (Pre-treat WT) and *Tlr4*^{-/-} (Pre-treat *Tlr4*^{-/-}) BMDMs that were collected following 6 hr of treatment in pre-treatment media, and in poly(I:C)-primed *Tlr4*^{-/-} BMDMs (Primed *Tlr4*^{-/-}). Data from two biologically independent samples are shown and are expressed as the regularized (r) log of the counts.

(B) WT BMDMs were treated for 1 hr with 1 μM TAK242 prior to, and during, overnight pre-treatment and subsequently stimulated with palmitate (1 mM for 4 hr) in the absence of TAK242.

(C and D) WT and *Tlr4*^{-/-} BMDMs were primed via overnight treatment with either Pam3CSK4 or poly(I:C) or remained unstimulated (Unprimed) followed by subsequent stimulation with either palmitate (1 mM for 4 hr) (C) or LPS (100 ng/mL for 0.5 hr) (D).

(E) BMDMs from C3H/HeN or C3H/HeJ mice were primed via overnight treatment with Pam3CSK4 or remained unstimulated (Unprimed) followed by subsequent stimulation with palmitate (1 mM for 4 hr).

The following numbers of biological replicates (independent mice) were used in each experiment: (A) = 2; (B) = 4; (C) = 4; (D) = 3; (E) = 4. All experiments were performed in either technical duplicates or triplicates and averaged such that for each independent experiment n = 1. All data are expressed as the mean ± SD and are expressed as a fold change. Symbols within bars represent the average value of each biological replicate. Asterisks represent statistical significance at the following α levels: ***p ≤ 0.001; **p < 0.01; *p < 0.05.

³H-palmitate esterification in pre-treated *Tlr4*^{-/-} BMDMs compared with WT BMDMs (Figures S6A and S6B). These effects were reversed in poly(I:C)-primed *Tlr4*^{-/-} BMDMs (Figures S6A and S6B). No differences were observed for ³H-palmitate uptake between WT, *Tlr4*^{-/-}, and poly(I:C)-primed *Tlr4*^{-/-} BMDMs (Figure S6C). These findings demonstrate that pre-treated WT and *Tlr4*^{-/-} BMDMs had a difference in their cellular metabolism, with pre-treated WT BMDMs being similar to M1 macrophages and pre-treated *Tlr4*^{-/-} BMDMs displaying an un-activated, or M0 phenotype. To confirm that the metabolism of lcSFAs is indeed required for their inflammatory actions, we inhibited long-chain fatty acyl-coenzyme A synthetase. Consistent with the idea that the metabolism of lcSFAs is a pre-requisite for their inflammatory effects, treatment of WT BMDMs with Triacsin C completely prevented palmitate-induced JNK activation in WT BMDMs (Figure 6A). mTOR is activated following TLR4 stimula-

tion and plays a critical role in the metabolic reprogramming that occurs in immune cells. Accordingly, to determine whether prior metabolic reprogramming via mTOR was required for lcSFA-induced inflammatory signaling, we pre-treated WT BMDMs with the mTOR inhibitor rapamycin for 1 hr prior to and during pre-treatment, before stimulation with palmitate in the absence of rapamycin. Consistent with the idea that TLR4-induced metabolic reprogramming is required for lcSFAs to initiate inflammatory signaling, inhibition of mTOR completely prevented palmitate-induced JNK activation (Figure 6B).

Given (1) that the metabolism of lcSFAs is required for their inflammatory actions; (2) that significant differences in cellular metabolism between WT, *Tlr4*^{-/-}, and poly(I:C)-primed *Tlr4*^{-/-} BMDMs exist; and (3) the importance of specific lipid species as well as the composition of the cellular lipidome more generally in mediating inflammatory responses, we hypothesized that

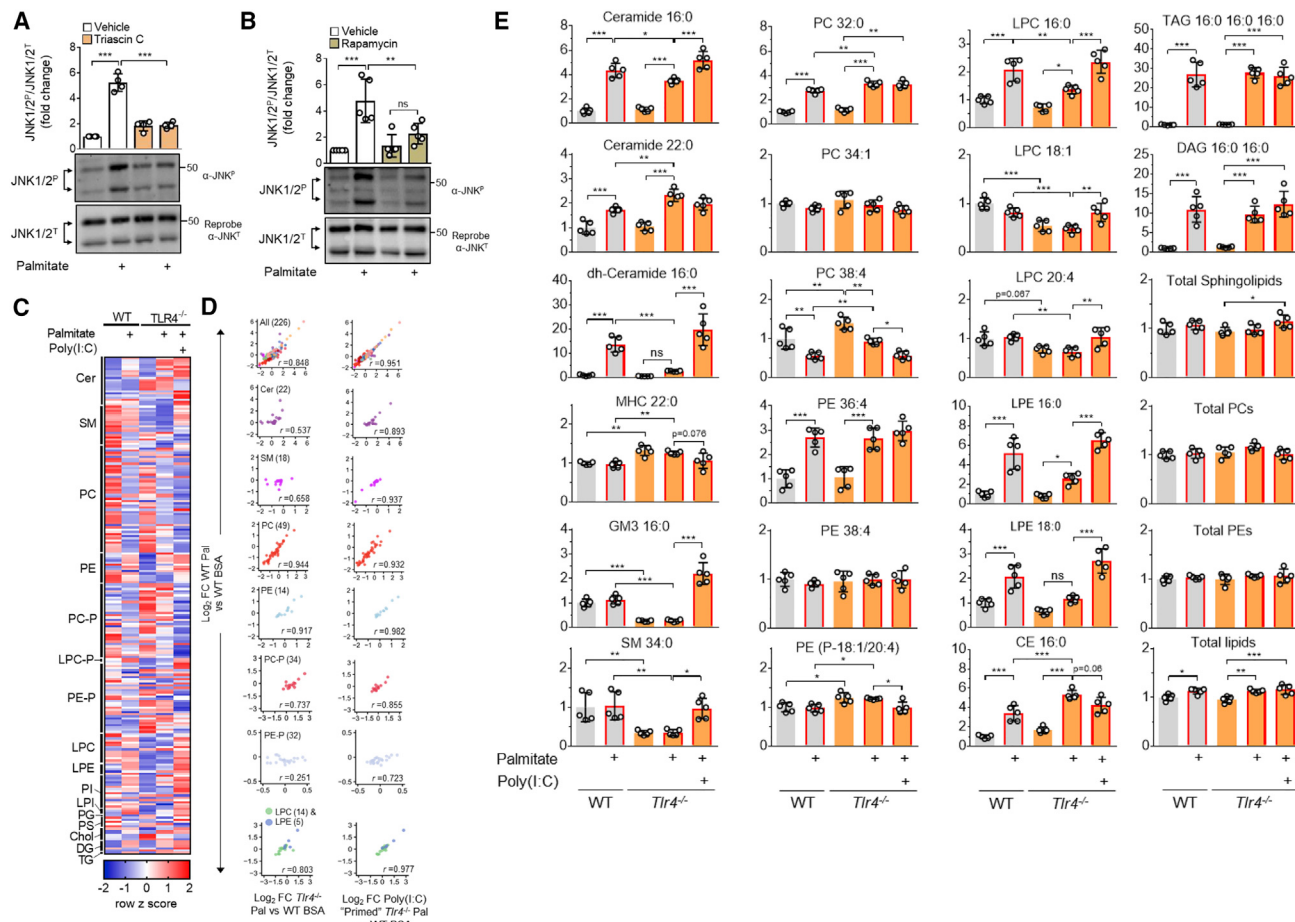


Figure 6. The Lipidome and Cellular Metabolism of *Tlr4*^{-/-} BMDMs Are Altered Compared with WT BMDMs and Are Normalized by Priming

(A and B) WT BMDMs were treated with palmitate (1 mM for 4 hr) in the presence or absence of Triacsin C (10 μ M; 1 hr prior to and during subsequent palmitate treatment) (A) or rapamycin (100 nM; co-incubated during overnight pre-treatment but not during palmitate treatment) (B). Cell lysates were analyzed by immunoblotting for levels of phosphorylated (^P) and total (^T) JNK1/2. Five and four, respectively, biological replicates (independent mice) were used in each experiment.

(C–E) WT and *Tlr4*^{-/-} BMDMs were stimulated with either palmitate (1 mM for 4 hr) or vehicle control following either standard overnight pre-treatment or priming with poly(I:C) and lipids analyzed by targeted mass spectrometry. Lipidomics analysis of all 226 detected lipids is shown as a heatmap (C). Z scores were calculated from the concentrations of individual lipid species. (D) Scatterplots and Pearson's product moment correlations (*r*) for all lipids as well as the indicated classes of lipids between palmitate-treated WT BMDMs and *Tlr4*^{-/-} BMDMs (left panels) and between palmitate-treated WT BMDMs and poly(I:C)-primed palmitate-stimulated *Tlr4*^{-/-} BMDMs (right panels). (E) Concentrations of the indicated lipid species. All values are shown as a fold change from WT BMDMs in the absence of palmitate (first column).

Data in (C)–(E) are from one experiment performed with five biological replicates (independent mice). Data in (A), (B), and (E) are expressed as the mean \pm SD. Symbols within bars represent the average value of each biological replicate. Asterisks represent statistical significance at the following α levels: *** p \leq 0.001; ** p $<$ 0.01; * p $<$ 0.05.

differences in the cellular lipidome between WT and *Tlr4*^{-/-} BMDMs may be a feature of the priming response, potentially underlying the sensitivity and insensitivity of WT and *Tlr4*^{-/-} BMDMs, respectively, to the inflammatory effects of palmitate. Using mass spectrometry-based lipidomics to determine the abundance of 226 lipid species, including abundant membrane lipids and neutral lipids, in WT, *Tlr4*^{-/-}, and poly(I:C)-primed *Tlr4*^{-/-} BMDMs, we observed three primary effects on the cellular lipidome: (1) lipids that were affected comparably in WT, *Tlr4*^{-/-}, and poly(I:C)-primed *Tlr4*^{-/-} BMDMs following palmitate treatment; (2) lipids that were not affected by palmitate treatment but were differentially abundant between WT and both

Tlr4^{-/-} and poly(I:C)-primed *Tlr4*^{-/-} BMDMs; and (3) lipid species that were differentially abundant between WT and *Tlr4*^{-/-} BMDMs, but not between WT and poly(I:C)-primed *Tlr4*^{-/-} BMDMs (Figures 6C–6E). In general, palmitate treatment resulted in a decrease in the abundance of phosphatidylcholines (PCs) and an increase in the abundance of numerous phosphatidylethanolamines (PEs) and ceramides in WT BMDMs, *Tlr4*^{-/-}, and poly(I:C)-primed *Tlr4*^{-/-} BMDMs (Figures 6C and 6E). The global lipidomes of palmitate-treated WT and *Tlr4*^{-/-} BMDMs demonstrated a strong positive relationship, indicating that the majority of changes in lipid abundance observed following palmitate treatment occurred independently of TLR4 expression

(Figure 6D, left panel; $r = 0.848$). This similarity in the overall global lipidome was largely due to similarities in the profiles of PCs and PEs (Figure 6D; $r = 0.944$ and 0.917 for PCs and PEs, respectively). For example, changes in the levels of PC 32:0 and PE 36:4, two of the most abundant species within PCs and PEs, while increasing markedly in response to palmitate treatment, were unaffected by the absence of TLR4 (Figure 6E). Notably, compared with PCs and PEs, the relationship between palmitate-treated WT and $Tlr4^{-/-}$ BMDMs for ceramides ($r = 0.537$), sphingomyelins ($r = 0.658$), and PE-plasmalogens ($r = 0.251$) was relatively dissimilar (Figure 6D), indicating that the absence of TLR4 altered the levels of lipid species within these particular classes of lipids. For example, levels of dihydroceramide 16:0, ceramide 16:0, GM3 16:0, and sphingomyelin 34:0 were altered in $Tlr4^{-/-}$ relative to WT BMDMs (Figure 6E). While a strong positive relationship was observed for lyso-PE/PC species between palmitate-treated WT and $Tlr4^{-/-}$ BMDMs (Figure 5B; $r = 0.803$), we noted that several lyso-PE/PC species were altered by the absence of TLR4, notably lyso-PC 16:0, lyso-PE 16:0, and lyso-PE 18:0 (Figure 6E).

Remarkably, priming $Tlr4^{-/-}$ BMDMs with poly(I:C) remodeled the global lipidome such that it was very similar to that of palmitate-treated WT BMDMs (Figures 6C–6E; $r = 0.848$ and $r = 0.951$ for palmitate-treated WT versus $Tlr4^{-/-}$ BMDMs and palmitate-treated WT versus poly(I:C)-primed $Tlr4^{-/-}$ BMDMs, respectively). Changes in the global lipidome following poly(I:C) priming were the result of alterations in the levels of lipids across nearly all lipid classes (Figure 6D), most notably ceramides, sphingomyelins, and PE-plasmalogens. PCs were the exception, being largely unaffected by priming ($r = 0.944$ versus $r = 0.932$ for palmitate-treated WT versus $Tlr4^{-/-}$ BMDMs and palmitate-treated WT versus poly(I:C)-primed $Tlr4^{-/-}$ BMDMs, respectively). For example, the reduced levels of dihydroceramide 16:0, ceramide 16:0, lyso-PC 16:0, lyso-PE 16:0, and lyso-PE 18:0 in palmitate-treated $Tlr4^{-/-}$ BMDMs were restored in poly(I:C)-primed $Tlr4^{-/-}$ BMDMs (Figure 6E). Similarly, the reduced levels of GM3 16:0, sphingomyelin 34:0, and LPC 18:1 and 20:4 observed in $Tlr4^{-/-}$ BMDMs were restored in poly(I:C)-primed $Tlr4^{-/-}$ BMDMs (Figure 6E). Finally, the levels of cholesterol ester 16:0, which were increased in palmitate-treated WT BMDMs and potentiated in $Tlr4^{-/-}$ BMDMs, were reduced to WT levels in poly(I:C)-primed $Tlr4^{-/-}$ BMDMs (Figure 6E), and the levels of triacylglycerol (16:0 16:0 16:0) and diacylglycerol (16:0 16:0) were unaltered between WT and $Tlr4^{-/-}$ BMDMs (Figure 6E). No differences were observed for the total (as calculated by summing all of the lipids within a given class) levels of PCs or PEs (Figure 6E). A small increase in total sphingolipids was observed in the poly(I:C)-primed $Tlr4^{-/-}$ BMDMs (Figure 6E).

TLR4 activation in Raw264.7 cells (transformed mouse macrophages) alters the expression of numerous genes in the sphingolipid metabolic network (KEGG [Kyoto Encyclopedia of Genes and Genomes]) (Köberlin et al., 2015). We observed a similar profile of gene expression changes, including, but not limited to, genes involved in *de novo* ceramide synthesis (*Sptlc1*, *Sptlc2*, and *Cers6*) and the processing of downstream sphingolipids (*Cerk*, *Sphk2*, *Ugcg*, and *St3gal5*) (Figure S6D). Similarly, genes within the glycerophospholipid metabolic network (KEGG) revealed an up- and downregulation of numerous genes in pre-treated WT BMDMs (Figure S6E). Differences in the expression

of genes within the sphingolipid and glycerophospholipid metabolic networks were abolished in $Tlr4^{-/-}$ BMDMs and recapitulated in poly(I:C)-primed $Tlr4^{-/-}$ BMDMs (Figures S6D and S6E). Comparison of RNA-seq and lipidomic data identified instances in which the expression of specific genes within the sphingolipid metabolic network was strongly associated with the abundance of the cognate sphingolipid—for example, *Cers6* with ceramide 16:0 and dihydroceramide 16:0, and *St3gal5* with GM3 16:0—underscoring the importance of prior transcriptional changes to subsequent alterations in the lipidome. Given the particularly strong differences in ceramide metabolism between WT and $Tlr4^{-/-}$ BMDMs, both at the transcriptomic and lipidomic level, we assessed whether palmitate-induced JNK activation was dependent on ceramide biosynthesis. However, myriocin and fenretinide, inhibitors of serine palmitoyl transferase, the rate-limiting enzyme in ceramide biosynthesis, and dihydroceramide desaturase, respectively, were without effect on palmitate-induced JNK activation (Figure S6F).

The lipid composition of cellular membranes influences the inflammatory potential of macrophages (Heinz et al., 2015; Köberlin et al., 2015; Rong et al., 2013; Wei et al., 2016), with alterations in the lipid composition of both the plasma membrane and ER membrane being linked to the activation of cell signaling pathways. In the case of the ER, alterations in the lipid composition of the ER membrane induce a process known as ER stress (Fu et al., 2011), while changes in the plasma membrane lipidome have recently been linked to the activation of Rho GTPases and Src family kinases (Wei et al., 2016). These membrane-initiated events ultimately culminate in the activation of JNK. Accordingly, we sought to determine the functional consequences of the above described alterations in the cellular lipidome by assessing palmitate-induced ER stress and the activation of Rho GTPases in WT and $Tlr4^{-/-}$ BMDMs. $Tlr4^{-/-}$ BMDMs were entirely protected from palmitate-induced ER stress, as determined by eIF2 α phosphorylation and the splicing of *Xbp1* (Figures 7A and 7B). Furthermore, priming of $Tlr4^{-/-}$ BMDMs with poly(I:C) completely restored palmitate-induced ER stress (Figure 7C). These data support the hypothesis that altered lipid metabolism contributes to protecting $Tlr4^{-/-}$ BMDMs against IcSFA-induced inflammation. In contrast, and despite complete inhibition of JNK activation (Figure 7D, right panel), palmitate treatment increased Rho GTPase activity comparably in WT and $Tlr4^{-/-}$ BMDMs (Figure 7D, left panel).

DISCUSSION

Herein, using a number of independent experimental approaches, we provide evidence that the IcSFA palmitate is not an agonist for TLR4. This finding challenges one of the central paradigms by which IcSFAs are believed to induce inflammation. In support of previously published studies, however, we also demonstrate that $Tlr4^{-/-}$ BMDMs are, indeed, protected from palmitate-induced inflammation. We reconcile these seemingly dichotomous findings by demonstrating that TLR-dependent priming of BMDMs is a pre-requisite for IcSFAs to induce inflammation.

While IcSFAs can activate inflammatory signaling in macrophages via a number of mechanisms, the activation of TLR4 by

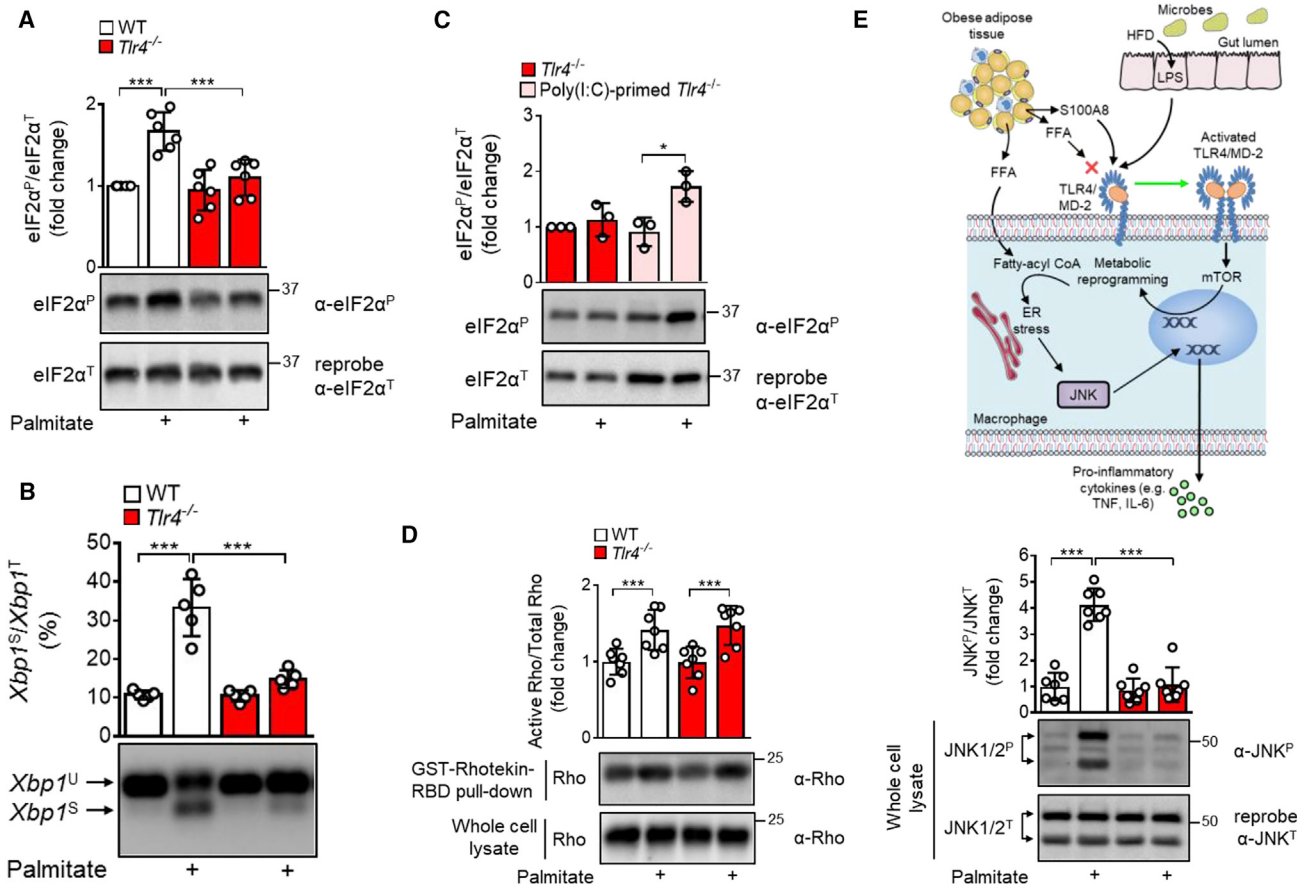


Figure 7. Deletion of TLR4 Prevents IcSFA-Induced Membrane Stress

(A–D) BMDMs from WT and *Tlr4*^{-/-} mice were stimulated with palmitate (1 mM for 4 hr) in the presence or absence of poly(I:C). Cell lysates were analyzed by immunoblotting for levels of phosphorylated (^P) and total (^T) eIF2 α (A and C). Unspliced (*Xbp1*^U) and spliced (*Xbp1*^S) forms of *Xbp1* were determined using conventional RT-PCR (B). Active Rho was detected following pull-down of active Rho (D) and cell lysates were analyzed by immunoblotting for levels of phosphorylated (^P) and total (^T) JNK.

(E) Model proposing how TLR4 becomes activated *in vivo* and how IcSFAs activate JNK.

The following numbers of biological replicates (independent mice) were used in each experiment: (A) = 6; (B) = 5; (C) = 3; (D) = 7. Experiments were performed in either technical duplicates or triplicates (A and B) or in singlet (C and D). All data are expressed as the mean \pm SD and are expressed as a fold change. Symbols within bars represent the average value of each biological replicate. Asterisks represent statistical significance at the following α levels: *** p < 0.001; * p < 0.05.

IcSFAs has become an important paradigm for understanding how obesity initiates inflammation, leading to dysregulated metabolism. Accordingly, while a wealth of previously published *in vitro* and *in vivo* studies support this concept, the lack of a clear structural basis for TLR4/MD-2 activation by IcSFAs, coupled with observations suggesting that IcSFAs are unlikely to be TLR4 agonists, prompted us to re-examine the concept that IcSFAs activate TLR4. Initially, using MD simulations, we show that palmitate does not productively engage TLR4/MD-2. We have previously used MD simulations to gain insight into the molecular signaling mechanism of TLR4/MD2 when in complex with a variety of agonists and antagonists (Paramo et al., 2013). Importantly, these previous computational experiments recapitulate numerous crucial aspects of the X-ray structure of TLR4/MD-2/LPS (Park et al., 2009), demonstrating both the validity of the simulation approach for examining TLR4/MD-2 activation as well as its application to identifying novel compounds with agonist/antagonist-like activities. While we did not observe

any agonist-like effects of palmitate in the present study, we cannot exclude the possibility that an alternate orientation or number of palmitate molecules, or potentially other SFAs, may satisfy the structural requirements necessary for TLR4/MD-2 activation. The recent discovery of a small molecule, Neoseptin-3, that bears no structural similarity to LPS but activates TLR4/MD-2 highlights the potential for TLR4/MD-2 to be activated in structurally diverse and unpredictable ways (Wang et al., 2016). While the mode of ligand binding to TLR4/MD-2 may be structurally distinct between agonists, the effect on the activation of downstream signaling pathways is highly stereotypical. Thus, while neoseptin-3 and LPS bear no structural similarity and their modes of TLR4/MD-2 engagement are somewhat distinct, their effects on the activation of downstream signaling pathways, including NF- κ B, JNK, and IRF3, are identical (Wang et al., 2016). In contrast, the IcSFA palmitate does not induce the same stereotypical rapid activation of JNK and NF- κ B that would be expected of a *bona fide* TLR4/MD-2 agonist.

The relatively late activation of JNK signaling by IcSFAs that we observed is consistent with numerous published studies. Moreover, we observed that palmitate was unable to induce the dimerization and endocytosis of TLR4, events that are absolutely fundamental to the activation of TLR4 signaling. Finally, inhibition of TLR4/MD-2 activation using LPS-Rs or TAK242, both of which prevent LPS-Ec-induced JNK activation, had no effect on palmitate-induced JNK activation. Collectively, these data provide compelling evidence that IcSFAs are not TLR4 agonists.

While alternate mechanisms of IcSFA-induced inflammation have been described (Hotamisligil, 2017; McNelis and Olefsky, 2014), there are nonetheless a large number of studies that identify a role for TLR4 in IcSFA- and obesity-induced inflammatory signaling. Importantly, consistent with this previous work, we observed a protective effect of TLR4 deficiency on IcSFA-induced JNK activation in two independent loss-of-function models, *Tlr4*^{-/-} mice and C3H/HeJ mice. While our results are consistent with previous work, they do not support a model in which IcSFAs directly activate TLR4. Accordingly, to account for the observations that IcSFAs are not TLR4 agonists but that IcSFA-induced inflammatory signaling is completely TLR4-dependent, we considered that TLR4-dependent priming may be necessary for IcSFAs to activate inflammatory signaling. We provide several lines of evidence to support this idea. First, by RNA-seq, we found that in WT BMDMs pre-treatment activated TLR4, leading to an increase in the expression of canonical TLR4-dependent inflammatory genes. Second, inhibiting TLR4-dependent priming with TAK242 prevented IcSFA-induced inflammation. Finally, priming of *Tlr4*^{-/-} BMDMs with agonists of alternate TLRs restored IcSFA-induced inflammation. Thus, in WT BMDMs, IcSFAs provide a “second hit” that activates inflammatory signaling following an initial TLR4-dependent priming signal. This scenario is somewhat analogous to activation of the Nlrp3 inflammasome, where inflammasome activation by numerous agents requires prior TLR-dependent priming, which increases the expression of critical inflammasome components (Lamkanfi and Dixit, 2014). These findings potentially resolve previous contradictions in the literature about the role of TLR4 in IcSFA-induced inflammation. Specifically, while the consensus in the field has been that IcSFAs are TLR4 agonists, compelling data have demonstrated that contamination of BSA preparations with LPS can account for the apparent activation of TLR4 by IcSFAs (Erridge and Samani, 2009). Our results support these findings, demonstrating that BSA-associated contaminants or endogenous TLR4 agonists present within serum activate TLR4. Importantly, however, the demonstration herein that acute pharmacological inhibition of TLR4 abolishes LPS-Ec-induced JNK activation, but not palmitate-induced JNK activation, confirms that IcSFAs per se do indeed activate inflammatory signaling. Somewhat serendipitously, the experimental design employed herein has allowed us to dissociate these two independent processes.

Our findings suggest that a primary mechanism by which priming renders BMDMs sensitive to the inflammatory effects of IcSFAs is by altering macrophage metabolism and, consequently, the cellular lipidome. While it is possible that changes to individual lipid species mediate sensitivity to IcSFA-induced inflammation, we consider it more likely that changes in overall membrane lipid composition are responsible for mediating the

sensitivity to IcSFAs, as suggested previously (Holzer et al., 2011). In support of this idea, systems biology approaches have recently identified the importance of membrane lipid composition on the inflammatory potential of macrophages (Kö-berlin et al., 2015) and IcSFAs or diets high in fat activate inflammatory signaling pathways via the incorporation of IcSFAs or their metabolites into cellular membranes (Fu et al., 2011; Holzer et al., 2011; Wei et al., 2016). In this regard, our results demonstrate that modulating ER stress-induced JNK activation may be one mechanism by which alterations in macrophage metabolism and the cellular lipidome alter the inflammatory potential of IcSFAs.

The findings presented herein provide insight into how TLR4 regulates obesity-induced inflammation *in vivo*. In healthy, insulin-sensitive adipose tissue, adipose tissue-resident macrophages display an alternatively activated or M2 state, and contribute to the regulation of lipid homeostasis and whole-body metabolism (Brestoff and Artis, 2015). In contrast, classically activated, or M1, macrophages predominate in obese, insulin-resistant adipose tissue, where they contribute to adipose tissue inflammation and whole-body metabolic dysfunction (Brestoff and Artis, 2015). The demonstration herein that TLR4-dependent priming of macrophages is required for the inflammatory effects of IcSFAs provides insight into how TLR4 is activated *in vivo*. It is currently hypothesized that IcSFAs activate TLR4, thereby polarizing macrophages toward the classically activated state and initiating adipose tissue inflammation and metabolic dysfunction. Our work provides compelling evidence that IcSFAs are not TLR4 agonists, but instead provide a second hit of activation that is dependent upon prior TLR4 activation. How might obesity stimulate TLR4-dependent priming of macrophages *in vivo*? Gut ecology has a pronounced effect on the inflammatory potential of the gut microbiota and consequently systemic inflammation (Sonnenburg and Backhed, 2016). Specifically, it has been shown that obesity and diets high in saturated fat alter the composition of the gut microbiota, increasing the intestinal absorption of gut-derived microbial products that lead to an increased concentration of circulating LPS, a process termed “metabolic endotoxemia” (Cani et al., 2007; Sonnenburg and Backhed, 2016). Importantly, metabolic endotoxemia initiates adipose tissue inflammation and macrophage activation in a manner dependent on intact signaling via TLR4/MyD88/TRIF (Caesar et al., 2015). Our demonstration that TLR4-dependent priming of macrophages is necessary for IcSFA-induced inflammation, together with published studies demonstrating the existence of a microbiome-TLR4/LPS-adipose tissue axis, leads us to propose a model in which metabolic endotoxemia, and not increased IcSFA concentrations, is the proximal stimulus inducing classically activated macrophages and adipose tissue inflammation. Alternatively, the production of endogenous TLR4 agonists from obese adipose tissue, such as S100A8, may provide a local priming signal (Nagareddy et al., 2014). However, once recruited to the adipose tissue, macrophages, as a result of priming-induced metabolic reprogramming, are likely to be highly sensitive to the inflammatory effects of IcSFAs, the concentrations of which are elevated in obese adipose tissue (Figure 7E). Our findings also explain why macrophages within healthy, insulin-sensitive adipose tissue do not become inflamed by the lipid-laden environment of the adipose tissue; i.e., in the

absence of a priming signal they are not intrinsically sensitive to the inflammatory effects of IgSFAs.

Limitations of the Study

Because of its well-established capacity to induce cellular inflammation and hypothesized role as a TLR4 agonist, in the present study we focused on whether the IgSFA palmitate induced macrophage activation via TLR4. While our studies provide compelling evidence that palmitate is unable to activate TLR4, it remains possible that other SFAs may have the capacity to activate TLR4. While we consider it unlikely, whether other fatty acids are able to productively engage TLR4 to induce inflammatory signaling should be investigated. Furthermore, our studies do not exclude the possibility that palmitate, or potentially other fatty acids, may bind to TLR4/MD-2 or CD14, an LPS-binding molecule important in TLR4 activation. As demonstrated herein, if SFAs such as palmitate are capable of binding to TLR4/MD-2, it does not lead to TLR4 activation; however, if such binding were to occur, it may potentially act in an antagonistic manner. In this regard, it was recently shown that specific oxidized phospholipids are able to bind CD14, and, rather than inducing activation of the TLR4 signaling pathway, inhibit TLR4 signaling (Zanoni et al., 2017). Finally, while we demonstrate that the metabolism of palmitate is necessary for its inflammatory effects, and that lipid metabolism and the accumulation of particular lipid species are altered by TLR-dependent priming, we did not identify the specific lipid species that mediate palmitate-induced JNK activation. However, specific lipid classes, or species within a given class, may not necessarily be responsible for the inflammatory effects of SFAs. Rather, the broader physiochemical effects of SFAs, resulting from their incorporation into cellular membranes, may mediate the inflammatory effects of SFAs. While this concept has been hypothesized previously (Holzer et al., 2011), recent work delineates a mechanism by which an increase in the saturated lipid content of the ER membrane leads to IRE1 activation, a hallmark of ER stress (Halbleib et al., 2017).

STAR METHODS

Detailed methods are provided in the online version of this paper and include the following:

- KEY RESOURCES TABLE
- CONTACT FOR REAGENT AND RESOURCE SHARING
- EXPERIMENTAL MODEL AND SUBJECT DETAILS
 - Mice and Generation of BMDM
- METHOD DETAILS
 - Molecular Dynamics Simulations
 - Immunoblotting
 - TLR4 Dimerization and Endocytosis
 - Rho Activity Assay
 - TNF ELISA
 - Mass Spectrometry Lipidomics
 - XBP1 Splicing
 - ³H-Palmitate Experiments
 - RNA-Seq
 - Reagents
- QUANTIFICATION AND STATISTICAL ANALYSIS
- DATA AND SOFTWARE AVAILABILITY

SUPPLEMENTAL INFORMATION

Supplemental Information includes seven figures and can be found with this article online at <https://doi.org/10.1016/j.cmet.2018.03.014>.

ACKNOWLEDGMENTS

This study was funded, in part, by the National Health and Medical Research Council (NHMRC) project grant no. 586636 to M.A.F. and G.I.L. and the Victorian Governments Operational Support Program. M.A.F. is a Senior Principal Research Fellow of the NHMRC (APP1116936). S.L.M. acknowledges funding from the Sylvia and Charles Vieret Foundation, HHMI-Wellcome International Research Scholarship, and Glaxosmithkline. We would also like to acknowledge the three anonymous reviewers for their constructive advice and suggestions.

AUTHOR CONTRIBUTIONS

G.I.L., K.G.L., H.L.K., S.R., J.W., N.A.M., G.P., M.K.S.L., S.L.M., E.E., J.R.W.C., P.T., N.B., and D.C.K. conducted experiments and performed analysis. G.I.L., N.A.B., and P.J.B. planned, conducted, and analyzed molecular simulation experiments. K.G.L. conducted and S.R., N.B., D.C.K., and M.E.D. analyzed RNA-seq experiments. G.I.L., G.P., J.W., N.A.M., and P.J.M. conducted and analyzed lipidomics experiments. S.L.M., S.G., and A.J.M. provided key reagents and contributed to experimental design. G.I.L. was responsible for drafting the first draft of the manuscript, which was then commented on by M.A.F. and P.J.B. prior to being sent to all other authors. G.I.L. and M.A.F. jointly conceived the project and coordinated all aspects of this work.

DECLARATION OF INTERESTS

The authors have no competing interests.

Received: June 23, 2017

Revised: December 22, 2017

Accepted: March 25, 2018

Published: April 19, 2018

REFERENCES

- Bjelkmar, P., Larsson, P., Cuendet, M.A., Hess, B., and Lindahl, E. (2010). Implementation of the CHARMM force field in GROMACS: analysis of protein stability effects from correction maps, virtual interaction sites, and water models. *J. Chem. Theory Comput.* 6, 459–466.
- Brestoff, J.R., and Artis, D. (2015). Immune regulation of metabolic homeostasis in health and disease. *Cell* 161, 146–160.
- Bussi, G., Donadio, D., and Parrinello, M. (2007). Canonical sampling through velocity rescaling. *J. Chem. Phys.* 126, 014101.
- Caesar, R., Tremaroli, V., Kovatcheva-Datchary, P., Cani, P.D., and Bäckhed, F. (2015). Crosstalk between gut microbiota and dietary lipids aggravates WAT inflammation through TLR signaling. *Cell Metab.* 22, 658–668.
- Cani, P.D., Amar, J., Iglesias, M.A., Poggi, M., Knauf, C., Bastelica, D., Neyrinck, A.M., Fava, F., Tuohy, K.M., Chabo, C., et al. (2007). Metabolic endotoxemia initiates obesity and insulin resistance. *Diabetes* 56, 1761–1772.
- Dobin, A., Davis, C.A., Schlesinger, F., Drenkow, J., Zaleski, C., Jha, S., Batut, P., Chaisson, M., and Gingeras, T.R. (2013). STAR: ultrafast universal RNA-seq aligner. *Bioinformatics* 29, 15–21.
- Erbay, E., Babaev, V.R., Mayers, J.R., Makowski, L., Charles, K.N., Snitow, M.E., Fazio, S., Wiest, M.M., Watkins, S.M., Linton, M.F., et al. (2009). Reducing endoplasmic reticulum stress through a macrophage lipid chaperone alleviates atherosclerosis. *Nat. Med.* 15, 1383–1391.
- Erridge, C. (2010). Endogenous ligands of TLR2 and TLR4: agonists or assistants? *J. Leukoc. Biol.* 87, 989–999.
- Erridge, C., and Samani, N.J. (2009). Saturated fatty acids do not directly stimulate Toll-like receptor signaling. *Arterioscler. Thromb. Vasc. Biol.* 29, 1944–1949.

- Essmann, U., Perera, L., Berkowitz, M.L., Darden, T., Lee, H., and Pedersen, L.G. (1995). A smooth particle mesh Ewald method. *J. Chem. Phys.* **103**, 8577–8593.
- Everts, B., Amiel, E., van der Windt, G.J., Freitas, T.C., Chott, R., Yarasheski, K.E., Pearce, E.L., and Pearce, E.J. (2012). Commitment to glycolysis sustains survival of NO-producing inflammatory dendritic cells. *Blood* **120**, 1422–1431.
- Fu, S., Yang, L., Li, P., Hofmann, O., Dicker, L., Hide, W., Lin, X., Watkins, S.M., Ivanov, A.R., and Hotamisligil, G.S. (2011). Aberrant lipid metabolism disrupts calcium homeostasis causing liver endoplasmic reticulum stress in obesity. *Nature* **473**, 528–531.
- Galic, S., Fullerton, M.D., Schertzer, J.D., Sikkema, S., Marcinko, K., Walkley, C.R., Izon, D., Honeyman, J., Chen, Z.P., van Denderen, B.J., et al. (2011). Hematopoietic AMPK beta1 reduces mouse adipose tissue macrophage inflammation and insulin resistance in obesity. *J. Clin. Invest.* **121**, 4903–4915.
- Gaujoux, R., and Seoighe, C. (2010). A flexible R package for nonnegative matrix factorization. *BMC Bioinformatics* **11**, 367.
- Halbleib, K., Pesek, K., Covino, R., Hofbauer, H.F., Wunnicke, D., Hanelt, I., Hummer, G., and Ernst, R. (2017). Activation of the unfolded protein response by lipid bilayer stress. *Mol. Cell* **67**, 673–684.e8.
- Heinz, L.X., Baumann, C.L., Koberlin, M.S., Snijder, B., Gawish, R., Shui, G., Sharif, O., Aspalter, I.M., Muller, A.C., Kandasamy, R.K., et al. (2015). The lipid-modifying enzyme SMPDL3B negatively regulates innate immunity. *Cell Rep.* **11**, 1919–1928.
- Hernandez, E.D., Lee, S.J., Kim, J.Y., Duran, A., Linares, J.F., Yajima, T., Muller, T.D., Tschoop, M.H., Smith, S.R., Diaz-Meco, M.T., et al. (2014). A macrophage NBR1-MEKK3 complex triggers JNK-mediated adipose tissue inflammation in obesity. *Cell Metab.* **20**, 499–511.
- Hess, B. (2008). P-LINCS: a parallel linear constraint solver for molecular simulation. *J. Chem. Theory Comput.* **4**, 116–122.
- Hess, B., Kutzner, C., van der Spoel, D., and Lindahl, E. (2008). GROMACS 4: algorithms for highly efficient, load-balanced, and scalable molecular simulation. *J. Chem. Theory Comput.* **4**, 435–447.
- Hoebe, K., Du, X., Geerget, P., Janssen, E., Tabata, K., Kim, S.O., Goode, J., Lin, P., Mann, N., Mudd, S., et al. (2003). Identification of Lps2 as a key transducer of MyD88-independent TIR signalling. *Nature* **424**, 743–748.
- Holzer, R.G., Park, E.J., Li, N., Tran, H., Chen, M., Choi, C., Solinas, G., and Karin, M. (2011). Saturated fatty acids induce c-Src clustering within membrane subdomains, leading to JNK activation. *Cell* **147**, 173–184.
- Hornig, T., Barton, G.M., Flavell, R.A., and Medzhitov, R. (2002). The adaptor molecule TIRAP provides signalling specificity for Toll-like receptors. *Nature* **420**, 329–333.
- Hoshino, K., Takeuchi, O., Kawai, T., Sanjo, H., Ogawa, T., Takeda, Y., Takeda, K., and Akira, S. (1999). Cutting edge: toll-like receptor 4 (TLR4)-deficient mice are hyporesponsive to lipopolysaccharide: evidence for TLR4 as the Lps gene product. *J. Immunol.* **162**, 3749–3752.
- Hotamisligil, G.S. (2017). Inflammation, metaflammation and immunometabolic disorders. *Nature* **542**, 177–185.
- Huang, S., Rutkowsky, J.M., Snodgrass, R.G., Ono-Moore, K.D., Schneider, D.A., Newman, J.W., Adams, S.H., and Hwang, D.H. (2012). Saturated fatty acids activate TLR-mediated proinflammatory signaling pathways. *J. Lipid Res.* **53**, 2002–2013.
- Huang, S.C., Everts, B., Ivanova, Y., O'Sullivan, D., Nascimento, M., Smith, A.M., Beatty, W., Love-Gregory, L., Lam, W.Y., O'Neill, C.M., et al. (2014). Cell-intrinsic lysosomal lipolysis is essential for alternative activation of macrophages. *Nat. Immunol.* **15**, 846–855.
- Humphrey, W., Dalke, A., and Schulter, K. (1996). VMD: visual molecular dynamics. *J. Mol. Graph.* **14**, 33–38, 27–38.
- Jaeschke, A., and Davis, R.J. (2007). Metabolic stress signaling mediated by mixed-lineage kinases. *Mol. Cell* **27**, 498–508.
- Jia, L., Vianna, C.R., Fukuda, M., Berglund, E.D., Liu, C., Tao, C., Sun, K., Liu, T., Harper, M.J., Lee, C.E., et al. (2014). Hepatocyte Toll-like receptor 4 regulates obesity-induced inflammation and insulin resistance. *Nat. Commun.* **5**, 3878.
- Kayagaki, N., Warming, S., Lamkanfi, M., Vande Walle, L., Louie, S., Dong, J., Newton, K., Qu, Y., Liu, J., Heldens, S., et al. (2011). Non-canonical inflammasome activation targets caspase-11. *Nature* **479**, 117–121.
- Kim, H.M., Park, B.S., Kim, J.I., Kim, S.E., Lee, J., Oh, S.C., Enkhbayar, P., Matsushima, N., Lee, H., Yoo, O.J., et al. (2007). Crystal structure of the TLR4-MD-2 complex with bound endotoxin antagonist Eritoran. *Cell* **130**, 906–917.
- Köberlin, M.S., Snijder, B., Heinz, L.X., Baumann, C.L., Fauster, A., Vladimer, G.I., Gavin, A.C., and Superti-Furga, G. (2015). A conserved circular network of coregulated lipids modulates innate immune responses. *Cell* **162**, 170–183.
- Koliwad, S.K., Streeter, R.S., Monetti, M., Cornelissen, I., Chan, L., Terayama, K., Naylor, S., Rao, M., Hubbard, B., and Farese, R.V., Jr. (2010). DGAT1-dependent triacylglycerol storage by macrophages protects mice from diet-induced insulin resistance and inflammation. *J. Clin. Invest.* **120**, 756–767.
- Lamkanfi, M., and Dixit, V.M. (2014). Mechanisms and functions of inflammasomes. *Cell* **157**, 1013–1022.
- Lampropoulou, V., Sergushichev, A., Bambouskova, M., Nair, S., Vincent, E.E., Loguinicheva, E., Cervantes-Barragan, L., Ma, X., Huang, S.C., Griss, T., et al. (2016). Itaconate links inhibition of succinate dehydrogenase with macrophage metabolic remodeling and regulation of inflammation. *Cell Metab.* **24**, 158–166.
- Lee, J.Y., Sohn, K.H., Rhee, S.H., and Hwang, D. (2001). Saturated fatty acids, but not unsaturated fatty acids, induce the expression of cyclooxygenase-2 mediated through Toll-like receptor 4. *J. Biol. Chem.* **276**, 16683–16689.
- Li, B., and Dewey, C.N. (2011). RSEM: accurate transcript quantification from RNA-seq data with or without a reference genome. *BMC Bioinformatics* **12**, 323.
- Liao, F., Andalibi, A., deBeer, F.C., Fogelman, A.M., and Lusis, A.J. (1993). Genetic control of inflammatory gene induction and NF-kappa B-like transcription factor activation in response to an atherogenic diet in mice. *J. Clin. Invest.* **91**, 2572–2579.
- Lien, E., Means, T.K., Heine, H., Yoshimura, A., Kusumoto, S., Fukase, K., Fenton, M.J., Oikawa, M., Qureshi, N., Monks, B., et al. (2000). Toll-like receptor 4 imparts ligand-specific recognition of bacterial lipopolysaccharide. *J. Clin. Invest.* **105**, 497–504.
- Love, M.I., Huber, W., and Anders, S. (2014). Moderated estimation of fold change and dispersion for RNA-seq data with DESeq2. *Genome Biol.* **15**, 550.
- MacKerell, A.D., Bashford, D., Bellott, M., Dunbrack, R.L., Evanseck, J.D., Field, M.J., Fischer, S., Gao, J., Guo, H., Ha, S., et al. (1998). All-atom empirical potential for molecular modeling and dynamics studies of proteins. *J. Phys. Chem. B* **102**, 3586–3616.
- Mariathasan, S., Newton, K., Monack, D.M., Vucic, D., French, D.M., Lee, W.P., Roose-Girma, M., Erickson, S., and Dixit, V.M. (2004). Differential activation of the inflammasome by caspase-1 adaptors ASC and Ipaf. *Nature* **430**, 213–218.
- Martinon, F., Petrilli, V., Mayor, A., Tardivel, A., and Tschopp, J. (2006). Gout-associated uric acid crystals activate the NALP3 inflammasome. *Nature* **440**, 237–241.
- Mata-Haro, V., Cekic, C., Martin, M., Chilton, P.M., Casella, C.R., and Mitchell, T.C. (2007). The vaccine adjuvant monophosphoryl lipid A as a TRIF-biased agonist of TLR4. *Science* **316**, 1628–1632.
- McNelis, J.C., and Olefsky, J.M. (2014). Macrophages, immunity, and metabolic disease. *Immunity* **41**, 36–48.
- Moon, J.S., Nakahira, K., Chung, K.P., DeNicola, G.M., Koo, M.J., Pabon, M.A., Rooney, K.T., Yoon, J.H., Ryter, S.W., Stout-Delgado, H., et al. (2016). NOX4-dependent fatty acid oxidation promotes NLRP3 inflammasome activation in macrophages. *Nat. Med.* **22**, 1002–1012.
- Nagareddy, P.R., Kraakman, M., Masters, S.L., Stirzaker, R.A., Gorman, D.J., Grant, R.W., Dragoljevic, D., Hong, E.S., Abdel-Latif, A., Smyth, S.S., et al. (2014). Adipose tissue macrophages promote myelopoiesis and monocytosis in obesity. *Cell Metab.* **19**, 821–835.
- Nguyen, M.T., Favelyukis, S., Nguyen, A.K., Reichart, D., Scott, P.A., Jenn, A., Liu-Bryan, R., Glass, C.K., Neels, J.G., and Olefsky, J.M. (2007). A subpopulation of macrophages infiltrates hypertrophic adipose tissue and is activated by

- free fatty acids via Toll-like receptors 2 and 4 and JNK-dependent pathways. *J. Biol. Chem.* 282, 35279–35292.
- Nosé, S., and Klein, M.L. (2006). Constant pressure molecular dynamics for molecular systems. *Mol. Phys.* 50, 1055–1076.
- O'Neill, L.A., Kishton, R.J., and Rathmell, J. (2016). A guide to immunometabolism for immunologists. *Nat. Rev. Immunol.* 16, 553–565.
- Ohto, U., Fukase, K., Miyake, K., and Satow, Y. (2007). Crystal structures of human MD-2 and its complex with antiendotoxic lipid IVa. *Science* 316, 1632–1634.
- Osborn, O., and Olefsky, J.M. (2012). The cellular and signaling networks linking the immune system and metabolism in disease. *Nat. Med.* 18, 363–374.
- Pal, D., Dasgupta, S., Kundu, R., Maitra, S., Das, G., Mukhopadhyay, S., Ray, S., Majumdar, S.S., and Bhattacharya, S. (2012). Fetuin-A acts as an endogenous ligand of TLR4 to promote lipid-induced insulin resistance. *Nat. Med.* 18, 1279–1285.
- Paramo, T., Piggot, T.J., Bryant, C.E., and Bond, P.J. (2013). The structural basis for endotoxin-induced allosteric regulation of the Toll-like receptor 4 (TLR4) innate immune receptor. *J. Biol. Chem.* 288, 36215–36225.
- Paramo, T., Tomasio, S.M., Irvine, K.L., Bryant, C.E., and Bond, P.J. (2015). Energetics of endotoxin recognition in the toll-like receptor 4 innate immune response. *Sci. Rep.* 5, 17997.
- Park, B.S., Song, D.H., Kim, H.M., Choi, B.S., Lee, H., and Lee, J.O. (2009). The structural basis of lipopolysaccharide recognition by the TLR4-MD-2 complex. *Nature* 458, 1191–1195.
- Parrinello, M., and Rahman, A. (1981). Polymorphic transitions in single crystals: a new molecular dynamics method. *J. Appl. Phys.* 52, 7182–7190.
- Poltorak, A., He, X., Smirnova, I., Liu, M.Y., Van Huffel, C., Du, X., Birdwell, D., Alejos, E., Silva, M., Galanos, C., et al. (1998). Defective LPS signaling in C3H/HeJ and C57BL/10ScCr mice: mutations in Tlr4 gene. *Science* 282, 2085–2088.
- Raghavan, B., Martin, S.F., Esser, P.R., Goebeler, M., and Schmidt, M. (2012). Metal allergens nickel and cobalt facilitate TLR4 homodimerization independently of MD2. *EMBO Rep.* 13, 1109–1115.
- Rong, X., Albert, C.J., Hong, C., Duerr, M.A., Chamberlain, B.T., Tarling, E.J., Ito, A., Gao, J., Wang, B., Edwards, P.A., et al. (2013). LXRs regulate ER stress and inflammation through dynamic modulation of membrane phospholipid composition. *Cell Metab.* 18, 685–697.
- Saberi, M., Woods, N.B., de Luca, C., Schenk, S., Lu, J.C., Bandyopadhyay, G., Verma, I.M., and Olefsky, J.M. (2009). Hematopoietic cell-specific deletion of toll-like receptor 4 ameliorates hepatic and adipose tissue insulin resistance in high-fat-fed mice. *Cell Metab.* 10, 419–429.
- Schott, W.H., Haskell, B.D., Tse, H.M., Milton, M.J., Piganelli, J.D., Choisy-Rossi, C.M., Reifsnyder, P.C., Chervonsky, A.V., and Leiter, E.H. (2004). Caspase-1 is not required for type 1 diabetes in the NOD mouse. *Diabetes* 53, 99–104.
- Shi, H., Kokoeva, M.V., Inouye, K., Tzameli, I., Yin, H., and Flier, J.S. (2006). TLR4 links innate immunity and fatty acid-induced insulin resistance. *J. Clin. Invest.* 116, 3015–3025.
- Shi, J., Zhao, Y., Wang, Y., Gao, W., Ding, J., Li, P., Hu, L., and Shao, F. (2014). Inflammatory caspases are innate immune receptors for intracellular LPS. *Nature* 514, 187–192.
- Sonnenburg, J.L., and Backhed, F. (2016). Diet-microbiota interactions as moderators of human metabolism. *Nature* 535, 56–64.
- Takashima, K., Matsunaga, N., Yoshimatsu, M., Hazeki, K., Kaisho, T., Uekata, M., Hazeki, O., Akira, S., Izawa, Y., and Ii, M. (2009). Analysis of binding site for the novel small-molecule TLR4 signal transduction inhibitor TAK-242 and its therapeutic effect on mouse sepsis model. *Br. J. Pharmacol.* 157, 1250–1262.
- Takeuchi, O., and Akira, S. (2010). Pattern recognition receptors and inflammation. *Cell* 140, 805–820.
- Tan, Y., Zanoni, I., Cullen, T.W., Goodman, A.L., and Kagan, J.C. (2015). Mechanisms of toll-like receptor 4 endocytosis reveal a common immune-evasion strategy used by pathogenic and commensal bacteria. *Immunity* 43, 909–922.
- Tong, A.J., Liu, X., Thomas, B.J., Lissner, M.M., Baker, M.R., Senagolage, M.D., Allred, A.L., Barish, G.D., and Smale, S.T. (2016). A stringent systems approach uncovers gene-specific mechanisms regulating inflammation. *Cell* 165, 165–179.
- Wang, Y., Su, L., Morin, M.D., Jones, B.T., Whitby, L.R., Surakkattula, M.M., Huang, H., Shi, H., Choi, J.H., Wang, K.W., et al. (2016). TLR4/MD-2 activation by a synthetic agonist with no similarity to LPS. *Proc. Natl. Acad. Sci. USA* 113, E884–E893.
- Wei, X., Song, H., Yin, L., Rizzo, M.G., Sidhu, R., Covey, D.F., Ory, D.S., and Semenkovich, C.F. (2016). Fatty acid synthesis configures the plasma membrane for inflammation in diabetes. *Nature* 539, 294–298.
- Weir, J.M., Wong, G., Barlow, C.K., Greeve, M.A., Kowalczyk, A., Almasy, L., Comuzzie, A.G., Mahaney, M.C., Jowett, J.B., Shaw, J., et al. (2013). Plasma lipid profiling in a large population-based cohort. *J. Lipid Res.* 54, 2898–2908.
- Wen, H., Gris, D., Lei, Y., Jha, S., Zhang, L., Huang, M.T., Brickey, W.J., and Ting, J.P. (2011). Fatty acid-induced NLRP3-ASC inflammasome activation interferes with insulin signaling. *Nat. Immunol.* 12, 408–415.
- Yamamoto, M., Sato, S., Hemmi, H., Hoshino, K., Kaisho, T., Sanjo, H., Takeuchi, O., Sugiyama, M., Okabe, M., Takeda, K., et al. (2003). Role of adaptor TRIF in the MyD88-independent toll-like receptor signaling pathway. *Science* 301, 640–643.
- Yamamoto, M., Sato, S., Hemmi, H., Sanjo, H., Uematsu, S., Kaisho, T., Hoshino, K., Takeuchi, O., Kobayashi, M., Fujita, T., et al. (2002). Essential role for TIRAP in activation of the signalling cascade shared by TLR2 and TLR4. *Nature* 420, 324–329.
- Zanoni, I., Ostuni, R., Marek, L.R., Barresi, S., Barbalat, R., Barton, G.M., Granucci, F., and Kagan, J.C. (2011). CD14 controls the LPS-induced endocytosis of Toll-like receptor 4. *Cell* 147, 868–880.
- Zanoni, I., Tan, Y., Di Gioia, M., Springstead, J.R., and Kagan, J.C. (2017). By capturing inflammatory lipids released from dying cells, the receptor cd14 induces inflammasome-dependent phagocyte hyperactivation. *Immunity* 47, 697–709.e3.

STAR★METHODS

KEY RESOURCES TABLE

REAGENT or RESOURCE	SOURCE	IDENTIFIER
Antibodies		
Phospho-SAPK/JNK	Cell Signaling Technology	Cat#9251; RRID: AB_331659
SAPK/JNK	Cell Signaling Technology	Cat#9252; RRID: AB_2250373
Phospho-SEK1/MKK4	Cell Signaling Technology	Cat#4514; RRID: AB_2140946
SEK1/MKK4	Cell Signaling Technology	Cat#9152; RRID: AB_330905
Phospho-NF- κ B p65	Cell Signaling Technology	Cat#3597; RRID: AB_390740
NF- κ B p65	Cell Signaling Technology	Cat#4764; RRID: AB_823578
I κ B α	Cell Signaling Technology	Cat#4812; RRID: AB_331288
Phospho-eIF2 α	Cell Signaling Technology	Cat#3597; RRID: AB_390740
eIF2 α	Cell Signaling Technology	Cat#9722; RRID: AB_2230924
α -tubulin	Sigma Aldrich	Cat# T5168; RRID: AB_477579
NLRP3	R&D Systems	Cat# MAB7578
Caspase 1(M-20)	Santa Cruz Biotechnology	Cat# sc-514; RRID: AB_2068895
ASC (n-15)	Santa Cruz Biotechnology	Cat#sc-22514-R; RRID: AB_2174874
Anti-Rabbit IgG-HRP	GE Healthcare	Cat# NA934V; RRID: AB_772206
Anti-Mouse IgG-HRP	GE Healthcare	Cat# NXA931; RRID: AB_772209
Anti-rat IgG-HRP	Santa Cruz Biotechnology	Cat# sc-2065; RRID: AB_631756
F4/80-FITC Clone BM8	BioLegend	Cat#123108; RRID: AB_893502
TLR4-PE-Cy7 Clone MTS510	BioLegend	Cat#117609; RRID: AB_2044019
TLR4-APC Clone SA15-21	BioLegend	Cat#145405; RRID: AB_2562502
Chemicals, Peptides, and Recombinant Proteins		
Palmitate	Sigma Aldrich	Cat# P0500
Palmitoleate	Sigma Aldrich	Cat# P9417
Myristate	Sigma Aldrich	Cat#M3128
Palmitelaic Acid	Santa Cruz Biotechnology	Cat# sc-281121
LPS-Ec	Invivogen	Cat# trl-eblps
LPS-Rs	Invivogen	Cat# trl-rslps
TAK242	Invivogen	Cat# trl-cl195
Pam3CSK4	Invivogen	Cat# trl-pms
Poly(I:C)	Invivogen	Cat# trl-picw
myriocin	Sigma Aldrich	Cat# M1177
fenreteride	Tocris	Cat#1396
Triascin C	Tocris	Cat#2472
Rapamycin	Tocris	Cat#1292
BSA	Sigma Aldrich	Cat#A6003
3-H-Palmitate	PerkinElmer	Cat# NET0430005MC
DMSO	Sigma Aldrich	Cat#D2650
Trizol	Invitrogen	Cat#15596026
TurboDNase	Invitrogen	Cat#AM2238
RPMI Glutamax	Gibo by life technologies	Cat#61870
Penicillin/Strep	Gibo by life technologies	Cat#15140
DTT	Sigma Aldrich	Cat#D0632
Phosphatase Inhibitor Cocktail 2	Sigma Aldrich	Cat#P5726
Protease Inhibitor Cocktail	Sigma Aldrich	Cat#P8340
SuperSignal West Pico Chemiluminescent Substrate	Thermo Scientific	Cat#34080

(Continued on next page)

Continued

REAGENT or RESOURCE	SOURCE	IDENTIFIER
SuperSignal West Femto Maximum Sensitivity Substrate	Thermo Scientific	Cat#34095
Ficoll-Paque	GE Healthcare	Cat#17-1440-03
Accutase	Sigma Aldrich	Cat#A6964
Critical Commercial Assays		
Rho activity assay	Cell Signaling Technology	Cat#8820
TNF ELISA	R&D Systems	Cat#DY410
Tetro cDNA synthesis kit	Bioline	Cat#BIO-65043
Qiagen RNeasy extraction kit	Qiagen	Cat#74104
Pierce BCA Protein Assay Kit	Thermo Scientific	Cat#23227
MACS Human Pan Monocyte Negative Selection Kit	Miltenyi Biotec	Cat#130-096-537
Deposited Data		
Raw and Analyzed data	This paper	GEO: GSE100526
Experimental Models: Organisms/Strains		
C57Bl6/J	AMREP Animal Facility, Melbourne	In house breeding
C3H/HeN	WEHI	In house breeding
C3H/HeJ	Animal Resources Centre, WA, Australia	In house breeding
<i>Tlr4</i> ^{-/-}	AMREP Animal Facility, Melbourne	In house breeding; Hoshino et al., 1999 .
<i>Nlrp3</i> ^{-/-}	WEHI	In house breeding; Martinon et al., 2006 .
<i>Pycard</i> ^{-/-}	WEHI	In house breeding; Mariathasan et al., 2004 .
<i>Casp1</i> ^{-/-}	WEHI	In house breeding; Schott et al., 2004 .
Oligonucleotides		
XBP1 F - 5'-ACACGCTTGGGAAT GGACAC-3'	Geneworks	N/A
XBP1 R - 5'-CCATGGGAAGATGTTC TGGG-3'	Geneworks	N/A
Software and Algorithms		
Quantity One	BioRad	N/A
GraphPad Prism 7.03	N/A	N/A
Multiquant	N/A	N/A
IBM SPSS Statistics 22	N/A	N/A
FlowJo Version 8.7	Tree Star	N/A

CONTACT FOR REAGENT AND RESOURCE SHARING

Further information and requests for resources and reagents should be directed to and will be fulfilled by the Lead Contact, Mark A. Febbraio (m.febbraio@garvan.org.au).

EXPERIMENTAL MODEL AND SUBJECT DETAILS

Mice and Generation of BMDM

WT (C57Bl6/J) and *Tlr4*^{-/-} ([Hoshino et al., 1999](#)) male mice on a C57Bl6/J background were maintained at the Alfred Medical Research and Education Precinct (AMREP), Melbourne, Australia. C3H/HeN and C3H/HeJ mice were obtained from the Walter and Eliza Hall Institute, Melbourne, Australia, and Animal Resources Centre, Western Australia, Australia, respectively. Bone marrow was obtained from *Nlrp3*^{-/-} ([Martinon et al., 2006](#)), *Pycard*^{-/-} ([Mariathasan et al., 2004](#)), and *Casp1*^{-/-} ([Schott et al., 2004](#)) mice on a C57Bl6/J background, as well as WT (C57Bl6/J) control male mice maintained at the Walter and Eliza Hall Institute, Melbourne, Australia. All mice were maintained on a 12 h:12 h light:dark cycle. All experimental procedures complied with national guidelines for care and use of laboratory mice and were approved by an institutional animal ethics committee (AMREP AEC). BMDM were generated by flushing the hind limbs of mice with RPMI to obtain bone marrow. Following culture at 1 million cells/ml overnight in T75 flasks or 10 cm dishes in RPMI + Glutamax, 20% L929-cell conditioned media (vol/vol), 15% FBS (vol/vol), and 1% penicillin/streptomycin (vol/vol) (collectively referred to as L-cell media (LCM)), 1 million or 0.5 million non-adherent cells were plated into 6- or 12-well plates, respectively.

After 3 nights of incubation, the volume in the well was doubled with the addition of fresh LCM. Cells were considered to be fully differentiated to BMDM after 7 days of incubation with LCM. On the day prior to experimentation, LCM was replaced with new media containing RPMI + Glutamax, 5% FBS, and, in experiments in which BMDM were to be treated with fatty acids, 2% BSA (wt/vol). On the day of experiment this media was replaced with that containing specific treatments or the appropriate vehicle control.

Generation of HMDM

To generate primary human macrophages, human monocytes were isolated from buffy coats obtained from healthy donors (Red Cross Blood Bank of Australia). Peripheral blood mononuclear cells were isolated using Ficoll-paque density gradient centrifugation, and human primary monocytes purified using the MACS Human Pan Monocyte Negative Selection Kit (Miltenyi Biotec) according to the manufacturer's instructions. The purity of isolated monocytes, assessed using CD14⁺/CD16⁺ expression via flow cytometry, was greater than 85%. Freshly isolated monocytes (1x10⁶ cells/ml) were re-suspended in culture medium (RPMI 1640 supplemented with 10% FBS, 1% NEAA, 100 IU/ml penicillin, 100 µg/ml streptomycin). These cells were incubated for 7 days with human M-CSF to stimulate the differentiation of monocytes to macrophages. On the day prior to experimentation, M-CSF-containing media was replaced with new media containing RPMI + Glutamax, 5% FBS, and, in experiments in which HMDM were to be treated with fatty acids, 2% BSA (wt/vol). On the day of experiment this media was replaced with that containing specific treatments or the appropriate vehicle control.

METHOD DETAILS

Molecular Dynamics Simulations

System Construction

To obtain starting configurations for the palmitate-bound TLR4 receptor complex, the capacity of MD-2 for different numbers of palmitate molecules was first determined in simulations of isolated MD-2. A system containing three palmitate molecules (3 x palmitic acid) was constructed based on the X-ray structure of human MD-2 bound to three co-crystallized endogenous myristate molecules (PDB: 2E56) (Ohto et al., 2007). The palmitate-bound MD-2 structure was subsequently superimposed via least-squares fitting onto the MD-2 template from the human TLR4/MD-2 X-ray structure (PDB: 3FXI) (Park et al., 2009), yielding an “active” MD-2-bound 3x palmitic acid system. Furthermore, a system containing six palmitate molecules (6 x palmitic acid) was constructed based on the LPS-bound TLR4₂/MD-2₂ X-ray structure (PDB: 3FXI) (Park et al., 2009). Placement of the palmitate molecules in both systems was guided by the bound myristate or LPS acyl tails, respectively, using PyMOL (<https://www.pymol.org>). The lipids in the 3x palmitic acid system bound to isolated MD-2 were well maintained during simulation, whereas in the 6x palmitic acid system, one of the palmitate molecules spontaneously exited the hydrophobic pocket of isolated MD-2. Thus, a 5x palmitic acid system was constructed and shown to be stable. Subsequently, the final coordinates from simulations of the 3x palmitic acid and 5x palmitic acid isolated MD-2 systems were extracted, and superimposed via least-squares fitting onto both MD-2 chains of the human TLR4₂/MD-2₂ X-ray structure (PDB: 3FXI) (Park et al., 2009). Finally, simulations were performed of the active TLR4₂/MD-2₂ complex in the presence of either three or five palmitate molecules.

Simulation Details

For all systems, the respective protein/ligand complex was placed in a truncated octahedral box with a minimum of 1.5 nm between solute and box edges, and solvated with explicit TIP3P waters with sufficient sodium and chloride ions to achieve overall neutrality to a 0.1 M concentration to mimic physiological salt conditions. Neutral pH was assumed and default ionization states were assigned to all ionizable residues. Energy minimization was performed using the steepest descent algorithm to remove any steric clashes between solute and solvent. Equilibration simulations totaling 1.5 ns were run in the *NpT* ensemble, and position restraints on protein/ligand heavy atoms were gradually released. Finally, production simulations were run for a minimum of 100 ns in the *NpT* ensemble. All simulations were performed using GROMACS version 4.6.5 (Hess et al., 2008) with the CHARMM22/CMAP forcefield (Bjelkmar et al., 2010; MacKerell et al., 1998). The protein, ligand, and solvent were separately maintained at 298 K using the velocity rescale thermostat (Bussi et al., 2007). The pressure was isotropically maintained at 1 bar using the Parrinello-Rhaman barostat (Nosé and Klein, 2006; Parrinello and Rahman, 1981). Electrostatic interactions were computed using smooth particle mesh Ewald (PME), with a real-space cutoff of 1.4 nm (Essmann et al., 1995). Lennard-Jones interactions were smoothly switched off between 1 nm and 1.4 nm. The neighbor list was updated every ten steps throughout the simulations and bond lengths were constrained using the P-LINCS algorithm (Hess, 2008), with a 2 fs integration time step for equations of motion.

Immunoblotting

For the quantification of the protein abundance BMDM were initially washed twice with ice cold PBS before the addition of ice cold lysis buffer (HEPES (20 mM), EGTA (2 mM), β-glycerophosphate (50 mM), DTT (0.1 mM), Na₃VO₄ (0.1 mM), NaF (1 mM), PMSF (1 mM), protease inhibitor cocktail (Sigma; P8340) and Phosphatase Inhibitor Cocktail 2 (Sigma; P5726)). Lysates were maintained on ice before being centrifuged at 16,000 g for 20 min at 4°C and the supernatant collected for subsequent determination of protein concentration via the BCA method (Thermo Scientific). 20 µg of total protein was solubilised in Laemmli buffer and heated at 95°C for 5 min. A molecular weight ladder was added to all gels (#161-0373; Bio-Rad). Proteins were resolved by SDS-polyacrylamide gel electrophoresis, transferred to 0.2 µm nitrocellulose membranes (Bio-Rad) by wet transfer at 4°C, washed in Tris-buffered Saline containing Tween 20 (TBST) for ~30 min, blocked in 5% skim milk for 1 h at room temperature, and washed for a further 30 min in TBST prior to incubation with primary antibodies. All antibodies were used at a concentration of 1:1000, with the exception of

α -tubulin which was used at 1:5000, and were made up in TBST + 2.5% (wt/vol) BSA + 0.01% (wt/vol) NaN_3 . After overnight incubation at 4°C membranes were washed for 30 min at room temperature in TBST, incubated with the appropriate secondary antibody for 1 h at room temperature, and washed for a further 30 min in TBST at room temperature before developing. Proteins were detected by chemiluminescence and specific bands quantified using Quantity One software (Bio-Rad).

TLR4 Dimerization and Endocytosis

TLR4 dimerization and endocytosis were assessed essentially as described in [Zanoni et al. \(2017\)](#). Briefly, WT BMDM were treated with LPS (1 $\mu\text{g}/\text{ml}$) or palmitate (1 mM) for 15 and 120 min at 37°C. Untreated control samples were also collected at 15 and 120 min. At the completion of the time points, BMDM were washed twice with cold PBS and detached with Accutase (A6964, Sigma-Aldrich). Cells were washed in FACS buffer (HBSS containing 0.05% BSA, 0.5 mM EDTA) and BMDM subsequently stained with antibodies against F4/80-FITC (Clone BM8, BioLegend) or TLR4 antibodies that assess dimerization (TLR4-PE-Cy7, clone MTS510, BioLegend) or endocytosis (TLR4-APC, Clone SA15-21, BioLegend) for 30 min on ice. Stained cells were washed with 1 ml FACS buffer, resuspended in 150 μl of FACS buffer, and surface staining analysed with BD Fortessa. The geometric mean fluorescence intensity of TLR4-APC and TLR-PE/Cy7 was recorded and the percentage dimerization and endocytosis of TLR4 calculated as described in [Zanoni et al. \(2017\)](#).

Rho Activity Assay

BMDM were grown in 10 cm dishes and treated as described above. Following 4 h of palmitate treatment BMDM were washed once with ice cold PBS and cells prepared essentially according to the manufacturer's instructions. After determining sample protein concentrations, samples were diluted to 1 mg/ml in Lysis/Binding/Wash buffer and 700 μg of total protein was loaded into the spin cup. To confirm the efficacy of the assay, the lysate from an untreated sample was treated *in vitro* with either GDP (to inactivate) or GTP γ S (to activate) for 15 min and these samples prepared in parallel with the experimental samples. As shown in [Figure S7](#), GTP γ S activated Rho compared with GDP.

TNF ELISA

Levels of TNF (DY410) in cell culture supernatants were assessed by DuoSet ELISA (R&D Systems) according to the manufacturer's instructions.

Mass Spectrometry Lipidomics

For mass spectrometry lipidomics, BMDM were grown in 6-well plates and washed twice with ice cold PBS following treatment. 200 μl of ice cold PBS was then added to each well and cells scraped from the plate. After sonication with a probe sonicator (Misonix ultrasonix liquid processor with Q Sonica CL5) for 15 s at ~17% amplitude protein concentrations were determined as described above. 40 μl (20 – 40 μg of protein) of this lysate was used for subsequent lipid extraction. Lipids were extracted and analysed by LC ESI-MS/MS using an Agilent 1200 liquid chromatography system and Applied Biosystems API 4000 Q/TRAP mass spectrometer with a turbo-ionspray source (350°C) and Analyst 1.5 and Multiquant data systems as described previously ([Weir et al., 2013](#)).

XBP1 Splicing

BMDM were grown in 6-well plates and washed twice with ice cold PBS following treatment. 1 ml of Trizol (Invitrogen) was added to each well and mRNA extracted according to the manufacturer's instructions. Total RNA measured using the ND-1000 NanoDrop Spectrophotometer (Thermo Scientific). Initial mRNA samples typically yielded low 260/230 ratios and samples were therefore subjected to ethanol precipitation in which 2.5 volumes of ice cold ethanol was added to samples, incubated at room temperature for 20 min, spun at 16,000 g for 15 min at 4°C, the supernatant removed, samples washed in 70% ethanol, air dried at 55°C, and resuspended in H₂O. cDNA was generated using the Tetro cDNA synthesis kit (Bioline). Unspliced (^U) and spliced (^S) XBP1 was amplified using primers (forward primer 5'-ACACGCTTGGGAATGGACAC-3' and reverse primer 5'-CCATGGGAAGATGTTCTGGG-3') under the following cycling conditions: 94°C for 4 min followed by 35 cycles of 94°C for 10 s, 68°C for 15 s, 72°C for 20 s, and a final 5 min at 72°C. PCR products were resolved on 2% agarose gels and visualised with ethidium bromide. Band densities were quantified (Quantity One Software) and the abundance of ^SXBP1 expressed as a % of total XBP1 (^UXBP1 + ^SXBP1).

³H-Palmitate Experiments

WT or *Tlr4*^{-/-} BMDM were pre-treated over-night in standard pre-treatment media (RPMI + Glutamax, 5% FBS, 2% BSA) or in pre-treatment media containing the TLR3 agonist poly(I:C) at a final concentration of 100 $\mu\text{g}/\text{ml}$. Following over-night pre-treatment, BMDM were treated with media containing both unlabelled palmitate (final concentration of 0.25 mM) and ³H-palmitate (final concentration of 5 μCi) for 12 h. We altered the conditions of palmitate treatment in these experiments for 2 reasons: (1) we increased the treatment time to 12 h to ensure sufficient palmitate oxidation such that we could detect the production of ³H₂O in the cell culture media; (2) prolonged treatment with higher concentrations of palmitate (e.g. 1 mM) causes cell toxicity, accordingly to minimise toxicity effects over the course of the treatment period we reduced the unlabelled palmitate concentration to 0.25 mM. To assess palmitate oxidation, an aliquot of the cell culture media was collected, spun to remove cell debris, added to a scintillation vial, and 5 ml of scintillation fluid (Irgasafe PLUS, PerkinElmer) added. To assess palmitate esterification, BMDM were washed twice in ice cold PBS, scraped in 200 μl of ice cold PBS, sonicated at 15% amplitude for 25 s, and lipids extracted in 2:1 chloroform/methanol.

A portion of the lipid-containing chloroform phase was then added to a scintillation vial, completely dried down under a stream of air, and 5 ml of scintillation fluid added. $^3\text{H}_2\text{O}$ and the incorporation of ^3H -palmitate into cellular lipid pools was determined by scintillation counting (Beckman Coulter, LS 6000 TA).

RNA-Seq

Libraries for RNA sequencing were prepared on the following samples: WT BMDM untreated, WT BMDM 6 h following media change to pre-treatment media, *Tlr4*^{-/-} BMDM untreated, *Tlr4*^{-/-} BMDM 6 h following media change to pre-treatment media, and *Tlr4*^{-/-} BMDM 6 h following media change to pre-treatment media that contained 100 μg Poly(I:C). RNA was prepared with Qiagen RNeasy extraction kit, DNase treated with TurboDNase (Life Technologies), confirmed DNA-free and RNA integrity was confirmed by Agilent 2100 Bioanalyzer (Agilent Technologies). Libraries were prepared with the TruSeq Stranded mRNA Sample Preparation Kit (Illumina). Sequencing was performed on HiSeq2500. The sequenced sample libraries were trimmed with Trim Galore (v.0.2.8), mapped to the mouse genome and transcriptome (Gencode mouse, v.M5) with STAR (v.2.4.0d) (Dobin et al., 2013), and counted with RSEM (v.1.2.12) (Li and Dewey, 2011). The counts reported with RSEM were normalized with R package DESeq2 (Love et al., 2014). Differentially expressed genes were calculated as those with FDR<0.05 and fold change > 1. Heatmaps were drawn using the aheatmap function from the NMF package for R, data is shown unscaled and clustered for rows (Gaujoux and Seoighe, 2010).

Reagents

All reagents used are listed in the [Key Resources Table](#). For all fatty acid experiments, stock fatty acids were made up in 100% ethanol at 100 mM and added to 0.22 μm -filter sterilised RPMI + Glutamax containing 5% FBS and 2% BSA at a final concentration of 0.0625 to 1 mM. To facilitate conjugation of fatty acids to BSA the mixture was incubated at 37°C for 30–45 min with gentle rocking. All TLR agonists (including LPS-Rs) were reconstituted with sterile water. TAK242, myriocin, fenretinide, Triascin C, and rapamycin were reconstituted in sterile DMSO.

QUANTIFICATION AND STATISTICAL ANALYSIS

Data were analysed by 1-way or 2-way analysis of variance, as appropriate, and post-hoc testing with correction for multiple comparisons was used to determine differences between specific groups. Statistical analysis was conducted using SPSS version 21 and GraphPad Prism Version 7. The similarity of cellular lipidomes between specific groups was assessed using the Pearson product-moment correlation co-efficient (r). The exact numbers of biological and technical replicates are stated in the figure legends. No methods were used for sample size determination or randomization.

DATA AND SOFTWARE AVAILABILITY

The accession number for the RNA-seq data reported in this paper is GEO: GSE100526.